Geobiology 2013 Lecture 6

Biogeochemical Tracers
Isotopics #3:
Biosynthetic fractionations and Intramolecular isotopic data, more of multi-element isotopics and the Precambrian C-Cycle

Acknowledgements: John Hayes, David DesMarais

Assigned Reading

- Hayes JM 2001 Fractionation of the isotopes of carbon and hydrogen in biosynthetic processes. Reviews in Mineralogy *Stable Isotopic Geochemistry*, John W. Valley and David R. Cole (eds.)
- David J Des Marais 1997. Isotopic evolution of the biogeochemical carbon cycle during the Proterozoic Eon Original Research Article, Organic Geochemistry, Volume 27, Issues 5–6, Pages 185-193

Revision of carbon isotopic principles

And examining isotopic fractionation at molecular, organismic and planetary scales

Isotope Effects

EQUILIBRIUM

$$^{13}CO_2\,(g) + H^{12}CO_3^-\,(aq) \rightleftharpoons {}^{12}CO_2\,(g) + H^{13}CO_3^-\,(aq)$$

$$K = \begin{matrix} 1.0092 & (0°C) \\ 1.0068 & (30°C) \end{matrix}$$

KINETIC

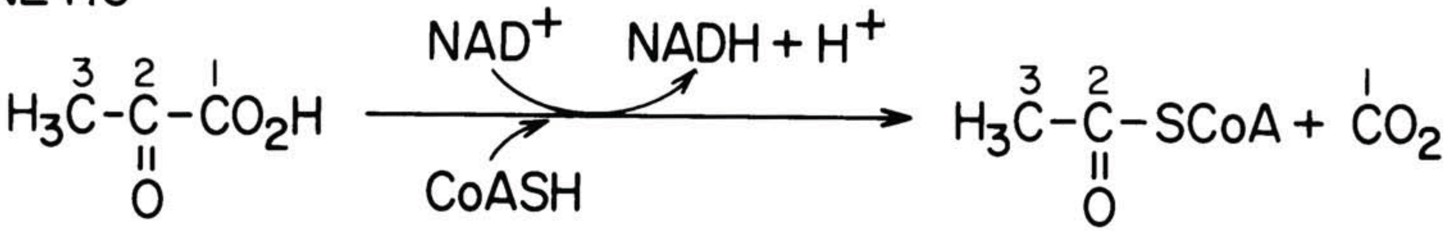

Pyruvate dehydrogenase

$$\left(\frac{^{12}k}{^{13}k}\right)_{C\text{-}2} = 1.0232$$

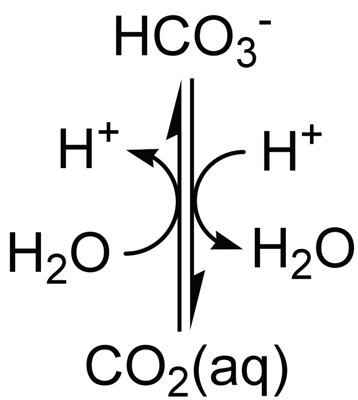

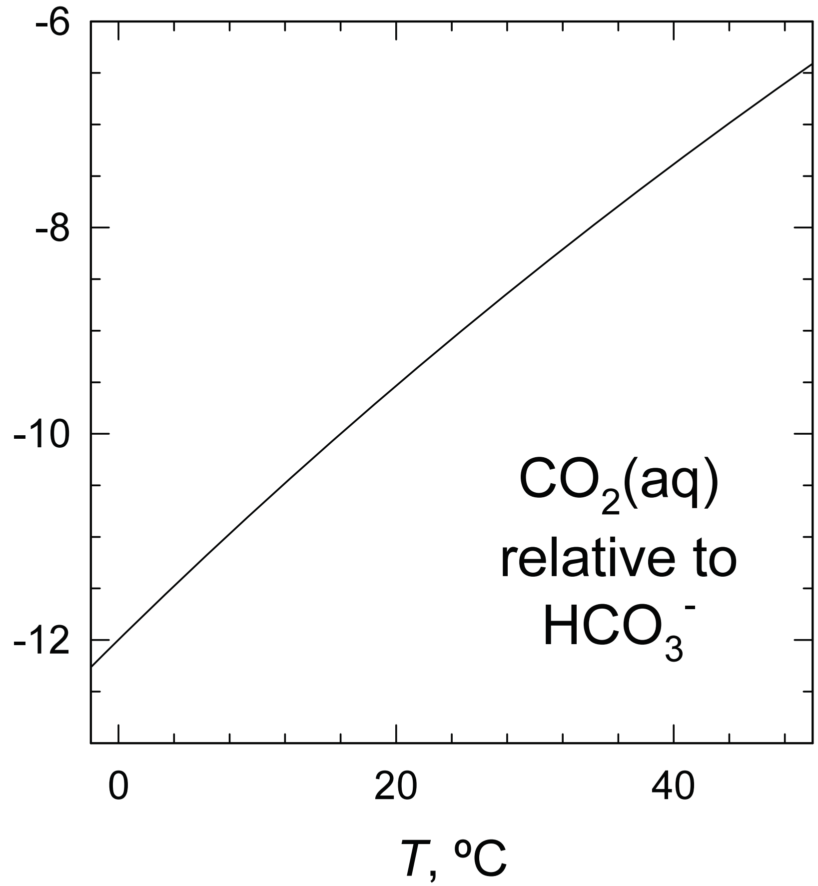

Mook *et al.*, 1974

$$R \equiv \frac{^{13}C}{^{12}C} \qquad \delta^{13}C = \frac{R_{sample}}{R_{VPDB}} - 1$$

Abundances of ^{13}C are reported in terms of δ. The zero point of the scale is defined by the VPDB standard.

Values of δ are commonly multiplied by 1000 and thus expressed in parts per thousand, ‰.

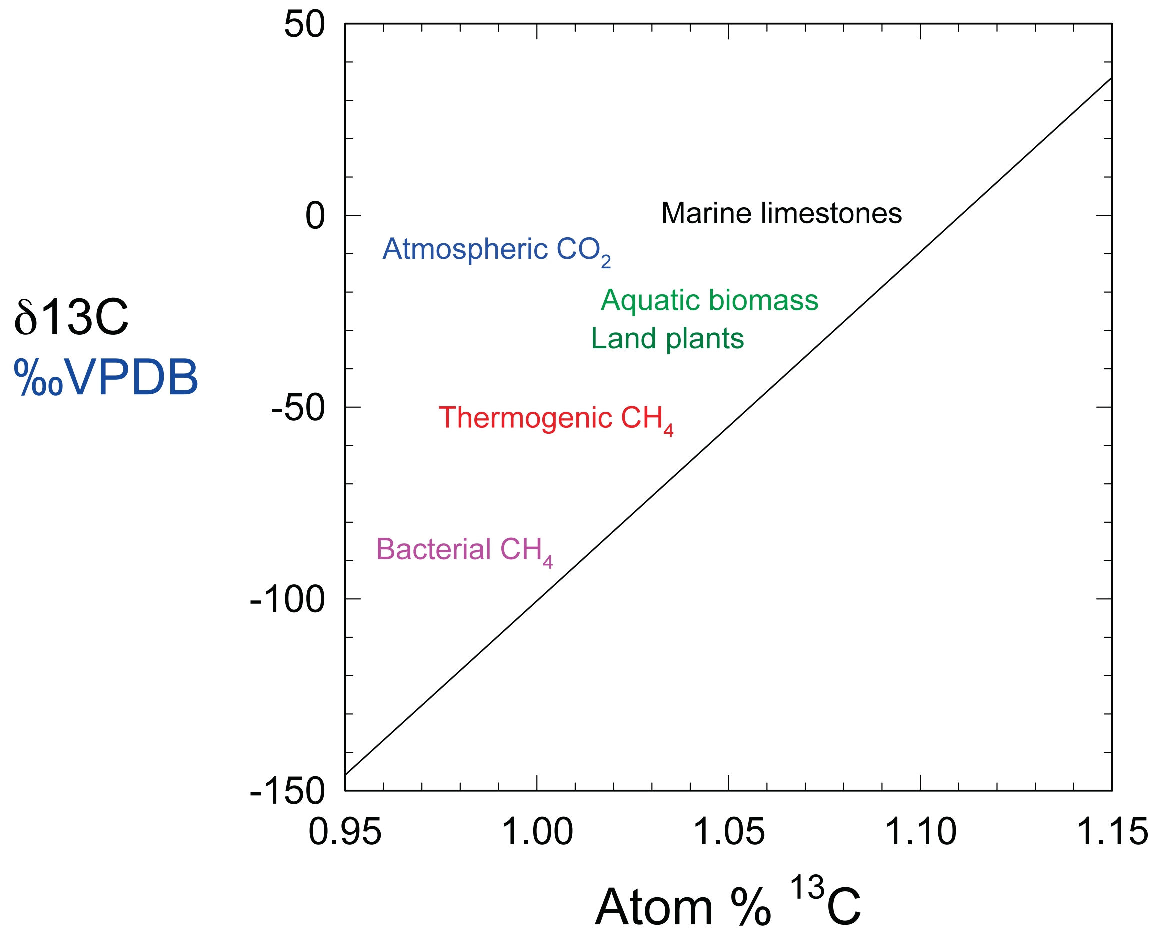

Isotope effects associated with biochemical reactions cause isotopic variations in nature

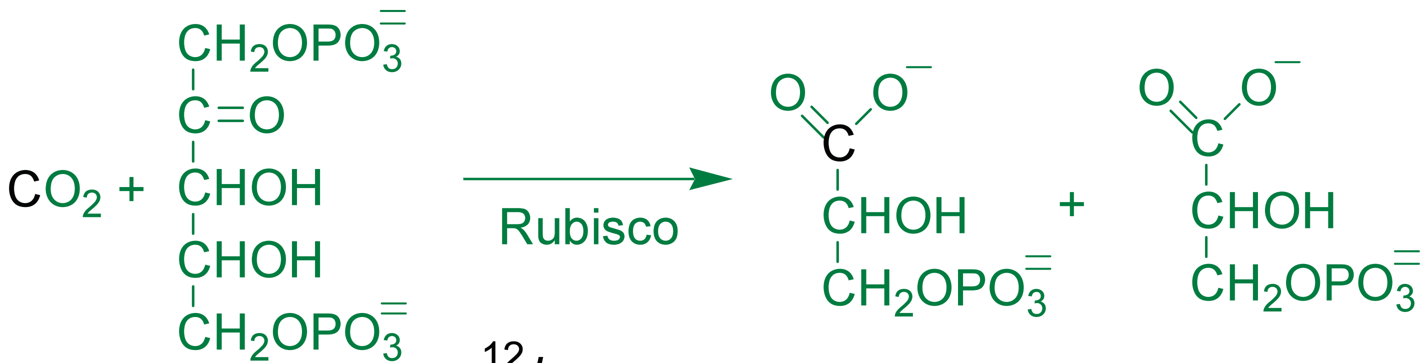

$$\frac{^{12}k}{^{13}k} \approx 1.029$$

Fixed C will be depleted in ^{13}C relative to CO_2

The relative depletion will be 29 parts per thousand

e. g., if CO_2 = 1.000% ^{13}C, fixed C = 0.971% ^{13}C

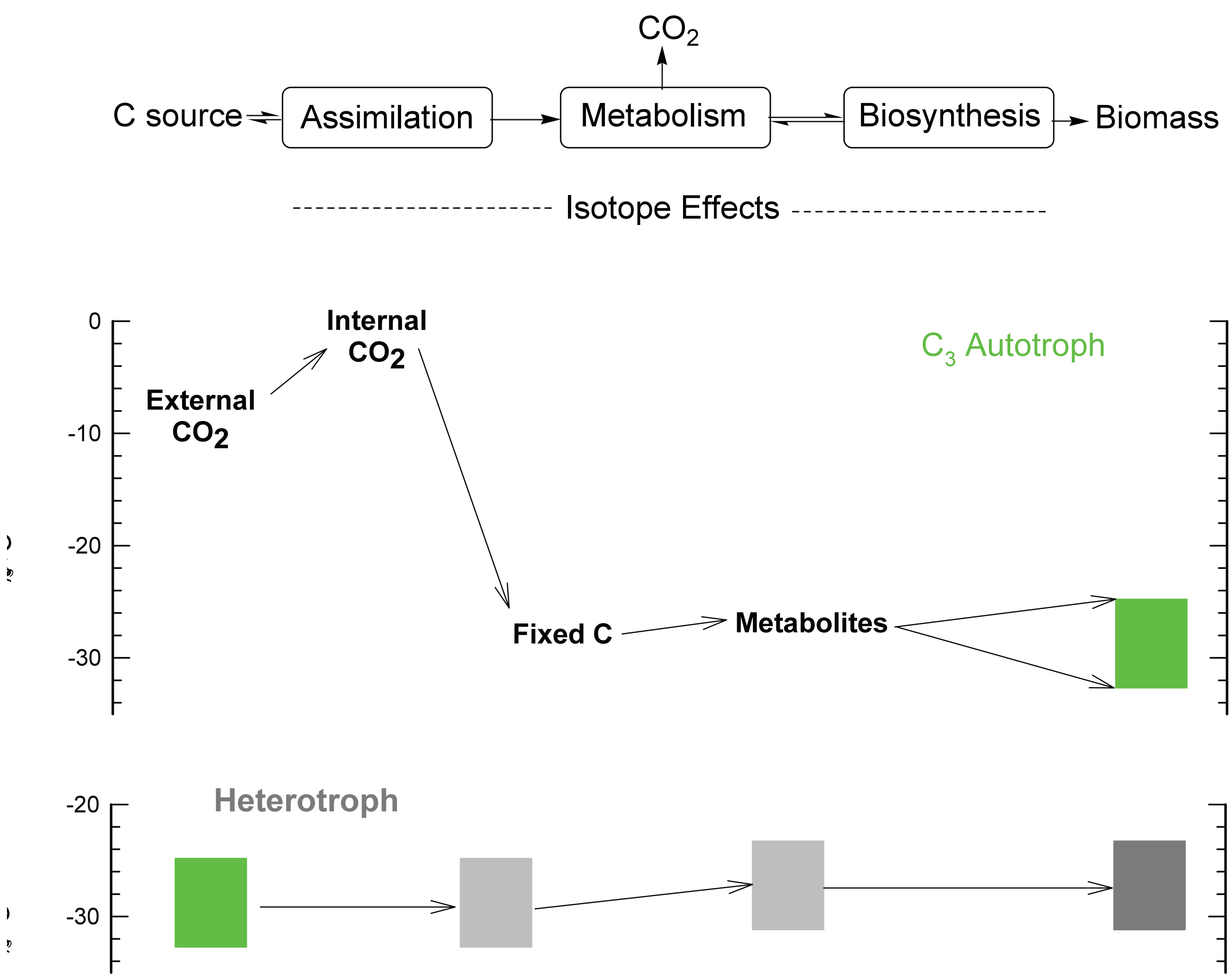
CO2
C source
Assimilation
Metabolism
Biosynthesis
Biomass
Isotope Effects
0
-10
-20
-30
Internal CO2
External CO2
C3 Autotroph
Fixed C
Metabolites
-20
-30
Heterotroph

Fractionation of C-Isotopes during Autotrophy

Pathway, enzyme	React & substr	Product	ε ‰	Organisms
C3			10-22	
Rubisco1	CO_2 +RUBP	3-PGA x 2	30	plants & algae
Rubisco2	CO_2 +RUBP	3-PGA x 2	22	cyanobacteria
PEP carboxylase	HCO_3^-+PEP	oxaloacetate	2	plants & algae
PEP carboxykinase	CO_2 +PEP	oxaloacetate		plants & algae
C4 and CAM			2-15	
PEP carboxylase	HCO_3^- +PEP CO_2 +RUBP	oxaloacetate	2	plants &
Rubisco1		3-PGA x 2	30	algae (C4)
Acetyl-CoA			15-36	bacteria
CO dehydrog	CO_2 + 2H+ CoASH	AcSCoA	52	
Pyruvate synthase	CO2 + Ac-CoA	pyruvate		
PEP carboxylase	HCO_3^-+PEP	oxaloacetate	2	
PEP carboxykinase	CO_2 +PEP	Oxaloacetate		
Reductive or reverse TCA	CO2 + succinyl-CoA (+ others)	α-ketoglutarate	4-13	Bacteria esp green sulfur
3-hydroxypropionate	HCO_3^- + acetylCoA	Malonyl-CoA		Green non-S

Carbon fixation (C4 & CAM pathways)

Formation of oxaloacetate from PEP (Phosphoenolpyruvate)
catalysed by PEP carboxylase

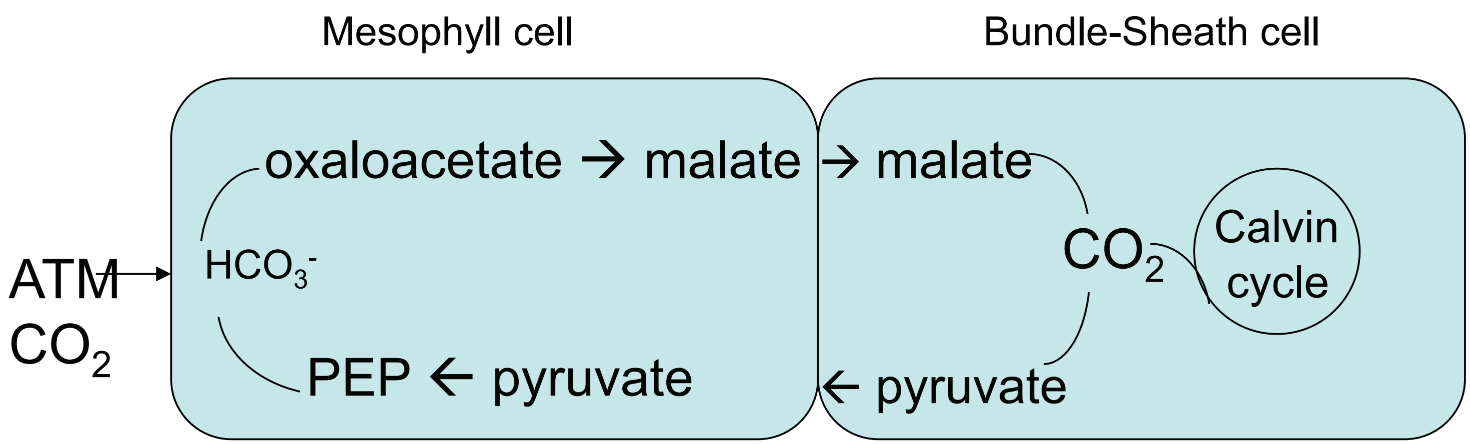

CAM (Crassulacean acid metabolism): Use both C3 and C4 metabolism separated in time

Isotopic consequences of different food sources

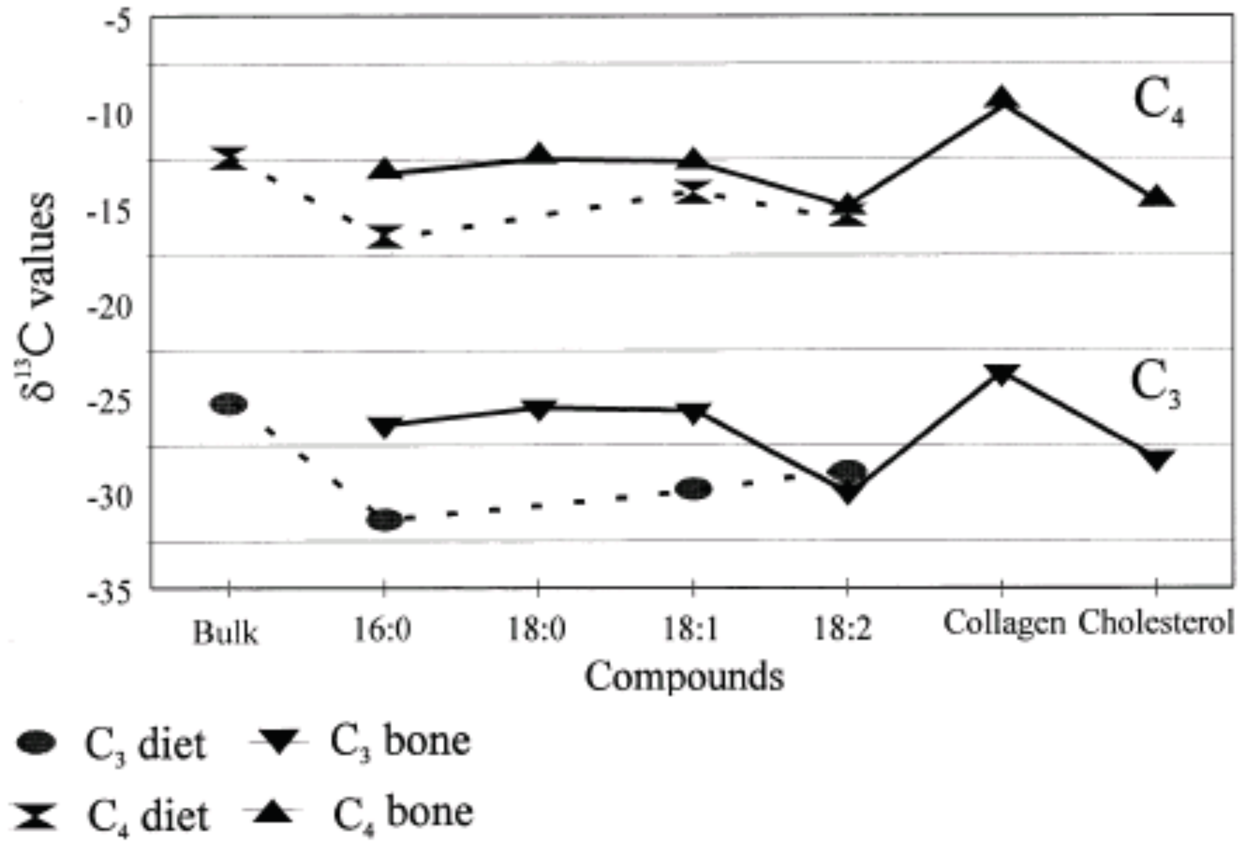

A. W. Stott, E. Davies, R. P. Evershed, & N. Tuross (1997) *Naturwissenschaften* **84**, 82–86.

Trophic Shifts

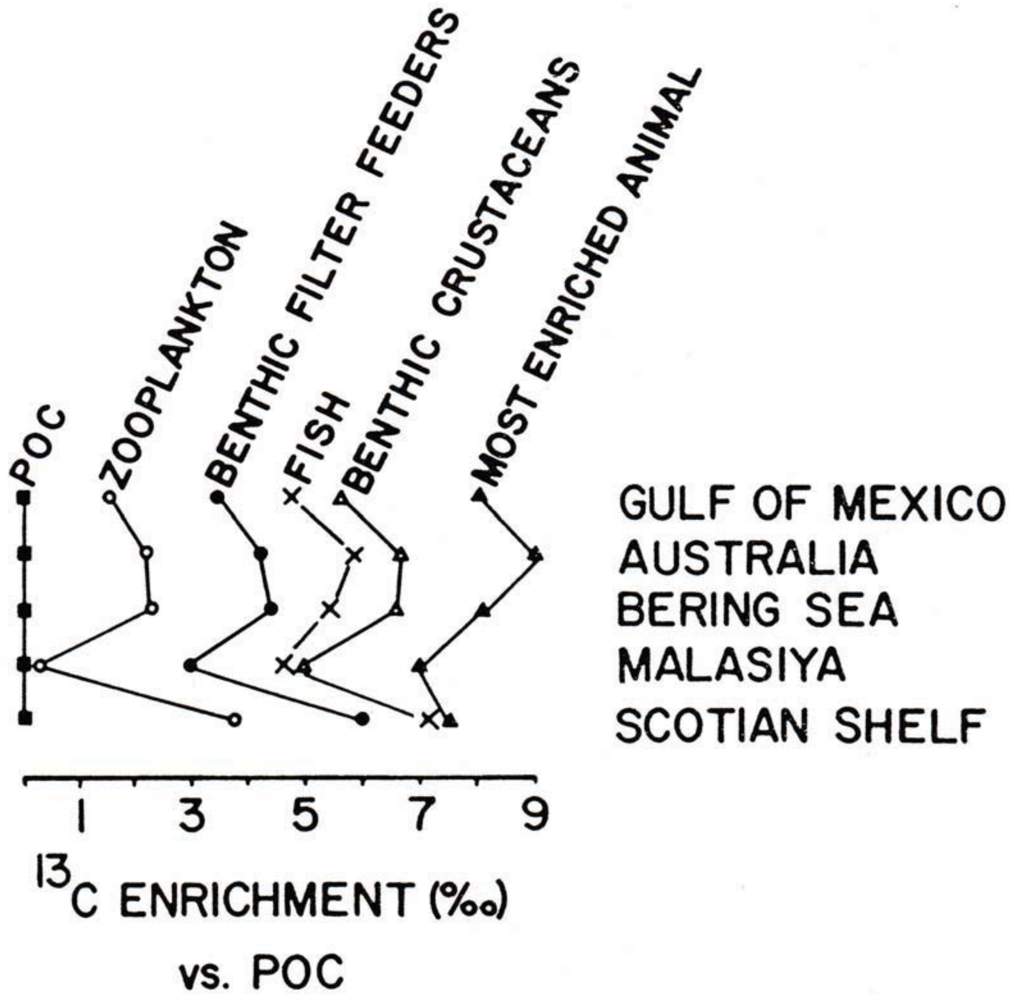

Intramolecular C-isotopic Differences
(DeNiro and Epstein, 1977; Monson and Hayes, 1980, 1982; reviewed Hayes, 2001)

Reactions occur between molecules but isotope selectivity is expressed as chemical bonds that are made or broken at particular carbon positions.

Isotope effects pertain to those specific positions and control fractionations only at that reaction site, not throughout the whole molecule.

To calculate changes in the isotopic compositions of whole molecules we must first calculate the change at the site and then allow for the rest of the molecule because the isotopic shift is diluted by mixing with carbon that is just along for the ride………………..Hayes, 2002

Compound Specific Isotope Analysis

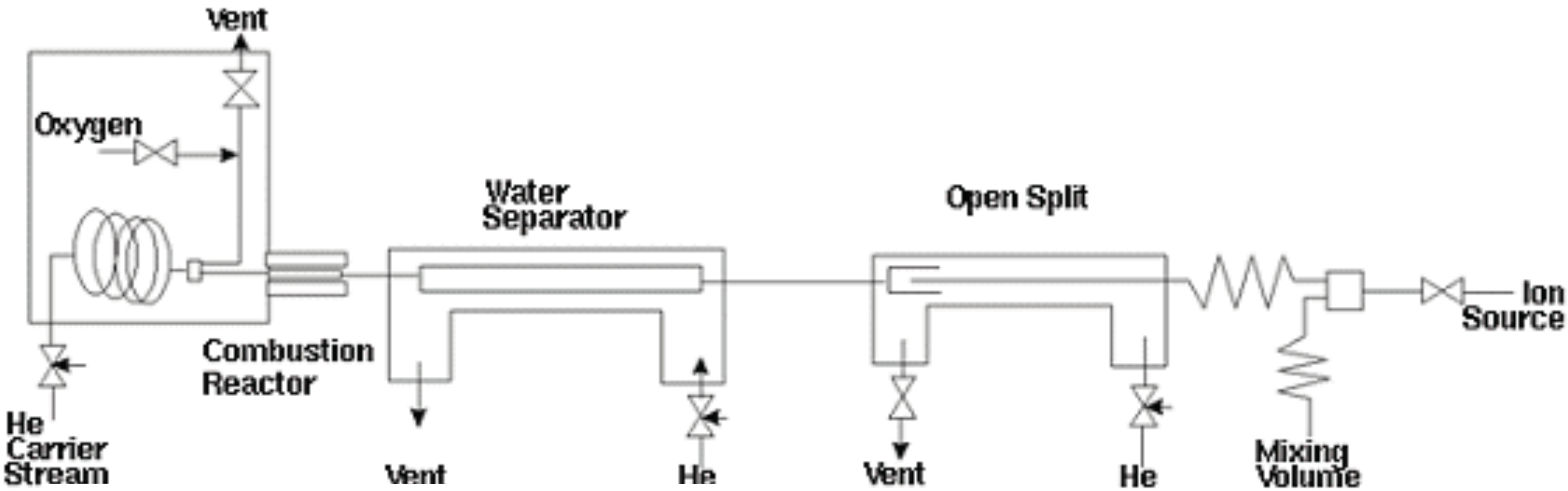

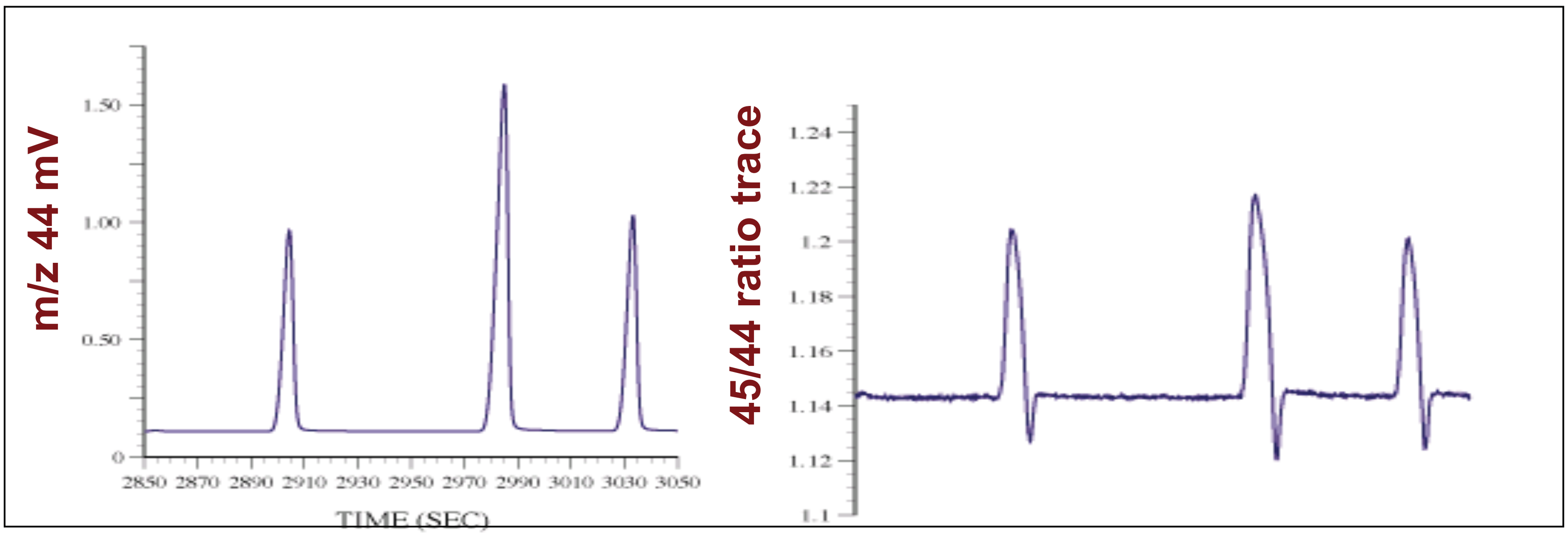

14. Argyle, E. *Icarus* **77**, 220–222 (1989).
15. O'Keefe, J. D. & Ahrens, T. J. in *Geological Implications of Impacts of Large Asteroid on the Earth, Geol. Soc. Am. Spec. Pap.* 190, 103–120 (1982).
16. Melosh, H. J. in *Geological Implications of Impacts of Large Asteroids and Comets* *Geol. Soc. Am. Spec. Pap.* 190, 121–127 (1982).
17. Kyte, F. T., Smit, J. & Wasson, J. T. *Earth planet. Sci. Lett.* **73**, 183–195 (1985).
18. Bohor, B. F., Triplehorn, D. M., Nichols, D. J. & Millard, H. T. *J. Geology* **15**, 896–89
19. Glasstone, S. & Dolan, P. J. *Effects of Nuclear Weapons* Table 7.40 (US Departmen and Energy, Washington, DC, 1977).
20. Bate, R. D., Mueller, D. D. & White, J. E. *Fundamentals of Astrodynamics* (Dover, New
21. Whipple, F. L. *Proc. Natn. Acad. Sci. U.S.A.* **36**, 687–695 (1950).
22. Brownlee, D. E. *A. Rev. Earth planet. Sci.* **13**, 147–173 (1985).
23. Chamberlain, J. W. & Hunten, D. M. *Theory of Planetary Atmospheres* 1–481 (Acad 1987).
24. Zahnle, K. J. in *Global Catastrophes, Geol. Soc. Am. Spec. Pap.* (in the press).
25. LaRocca, A. L. in *The Infrared Handbook* (eds Wolfe, W. L. & Zissis, G. J.) 5.1–5.
Naval Research, Alexandria, Virginia 1978).
26. Holton, J. R. *Introduction to Dynamic Meteorology* 2nd edn, 1–391 (Academic, New
27. Hildebrand, A. R. & Wolbach, W. S. *Lunar planet. Sci. Conf. XX* (abstr.) 414–415 (
28. Martin, S. *Proc. 10th Symp. (Int.) on Combustion* 877–896 (Williams and Wilkins, Bal
29. Simms, D. L. & Law, M. *Combust. Flame* **11**, 377–388 (1967).
30. Simms, D. L. *Combust. Flame* **7**, 253–261 (1963).
31. Argyle, E. *Science* **234**, 261 (1986).

ACKNOWLEDGEMENTS. We thank A. Hildebrand for discussion of the K/T boundary-la and petrology, D. Grinspoon for discussion early in this study, R. Selkirk for informat and G. Shoemaker for comments.

Evidence from carbon isotope measurements for diverse origins of sedimentary hydrocarbons

Katherine H. Freeman*, J. M. Hayes*, Jean-Michel Trendel† & Pierre Albrecht†

* Biogeochemical Laboratories, Departments of Chemistry and of Geology, Geology Building, Indiana University, Bloomington, Indiana 47405-5101, USA
† Laboratoire de Chimie Organique des Substances Naturelles, Départment de Chimie, Université Louis Pasteur, 1 rue Blaise Pascal, 67008 Strasbourg, France

TABLE 1 Carbon isotopic compositions of individual compounds

Peak	t_R* (s)	Amount† (nmol C)	$\delta^{13}C$‡ (‰)	Identification
1	1,679	1.1	-22.7 ± 1.0	norpristane
2	1,722	1.0	-30.2 ± 0.3	C_{19} acyclic isoprenoid
3	1,812	0.7	-25.4 ± 1.0	pristane
4	2,040	2.0	-31.8 ± 0.8	phytane
5	2,602	1.0	-29.1 ± 0.6	C_{23} acyclic isoprenoid
6	3,161	1.3	-23.9 ± 0.6	10β(H)-des-*A*-lupane
7	3,571	1.3	-24.9 ± 1.0	mixture of hydrocarbons
8	3,688	2.6	-73.4 ± 1.3	C_{32} acyclic isoprenoid
9	3,883	0.9	-24.2 ± 1.2	isoprenoid alkane
10	3,957	6.8	-49.9 ± 1.1	17β(H)-22,29,30-trisnorhopane
11	3,977	2.0	-60.4 ± 1.8	isoprenoid alkane
12	4,100	1.6	-43.5 ± 1.0	17α(H),21β(H)-30-norhopane
13	4,156	2.0	~ -45	17β(H),21α(H)-30-norhopane§
14	4,210	2.9	~ -34	17α(H),21β(H)-hopane‖
15	4,256	6.2	-65.3 ± 1.4	17β(H),21β(H)-30-norhopane
16	4,364	1.8	-39.4 ± 0.8	17α(H),21β(H)-homohopane
17	4,392	1.3	-35.2 ± 1.4	17β(H),21β(H)-hopane
18	4,552	4.2	-36.6 ± 0.5	17β(H),21β(H)-homohopane
19	4,692	15.4	-20.9 ± 0.5	lycopane¶
20	5,010	0.5	-27.0 ± 0.4	unknown hydrocarbon
21	5,408	0.8	-28.8 ± 1.0	unknown hydrocarbon

C-isotopic Composition of Individual Organic Compounds

Three major controls

- Source of carbon and its C-isotopic composition
- Fractionation during assimilation (eg heterotrophy, photosynthesis, methanotrophy)
- Fractionation during biosynthesis (lipids)

C-isotopic Composition of Organic Compounds

Source of carbon and its C-isotopic composition

- Inorganic carbon
  - (-7‰ atm. CO_2) assimilated by photosynthesis

    $\varepsilon \rightarrow$ 5-35 per mil depending on pathway extent of consumption

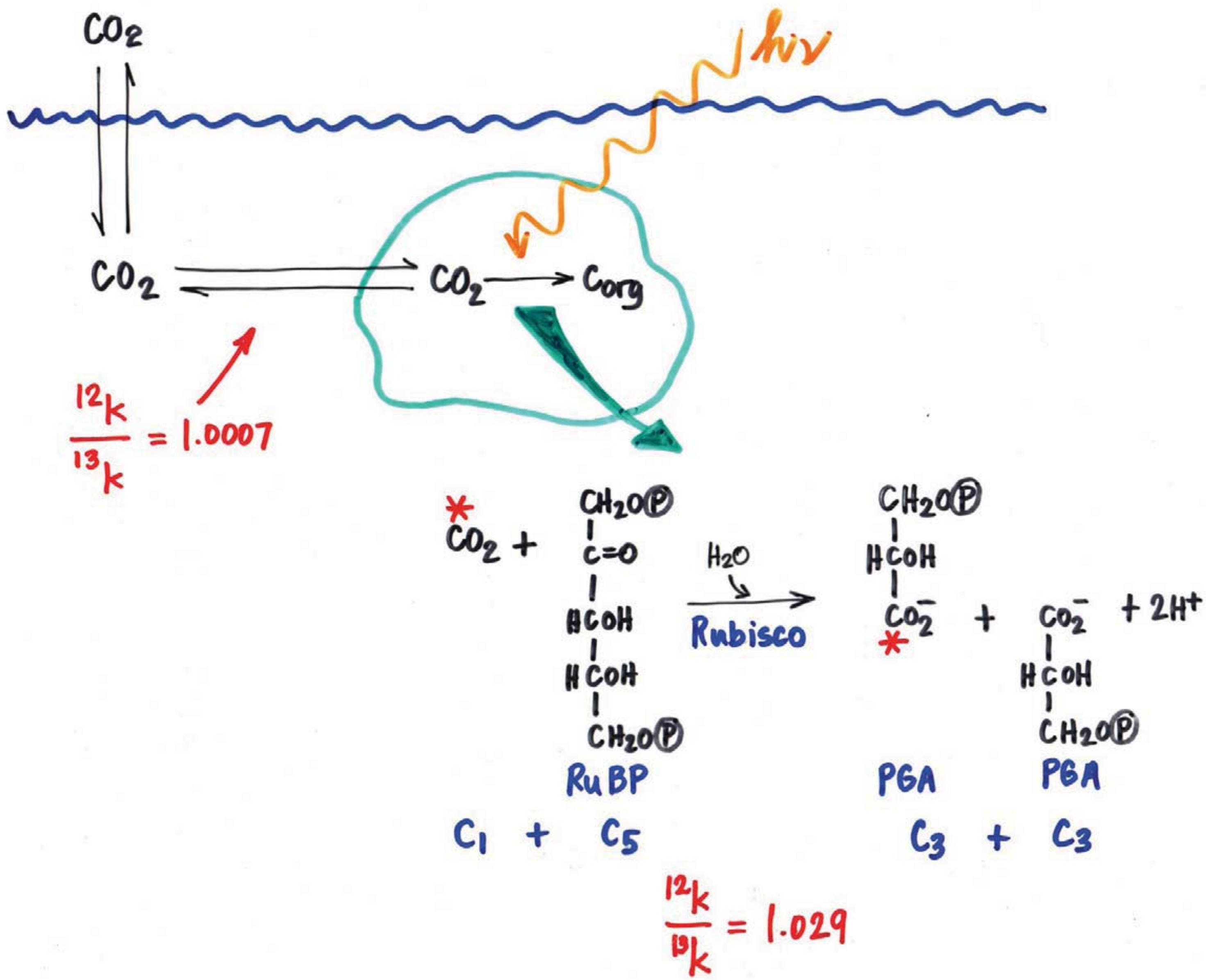
CO_2
$h\nu$
CO_2
CO_2
Corg
$\frac{^{12}k}{^{13}k} = 1.0007$
$^*CO_2$ +
$CH_2O(P)$
C=O
HCOH
HCOH
$CH_2O(P)$
RuBP
H_2O
Rubisco
$CH_2O(P)$
HCOH
CO_2^-
+
CO_2^-
HCOH
$CH_2O(P)$
$+ 2H^+$
PGA
PGA
C_1 + C_5
C_3 + C_3
$\frac{^{12}k}{^{13}k} = 1.029$

C-isotopic Composition of Individual Organic Compounds

Source of carbon and its C-isotopic composition

- Inorganic carbon
  - (-7‰ atm. CO_2) assimilated by photosynthesis

    ε → 5-35 per mil depending on pathway extent of consumption

- Organic carbon
  - (-25‰ on average) assimilated during heterotrophy

    ε → -1 (you are what you eat plus 1 per mil!!)

- Methane carbon
  - (-30 to -100‰) assimilated during methanotrophy

    ε → 0-30 per mil depending on pathway and extent of consumption http://www.astrobio.net/news/modules.php?op=modload&name=News&file=article&sid=34

Image removed due to copyright restrictions.

Café Methane

Image removed due to copyright restrictions.

At the very edge of the brine pool, the mussels are especially abundant and happy. This area is often filled with newly settled baby mussels perched on the shells of larger mussels just above the brine.
Credit: Penn State University, Dept. of Biology

Image removed due to copyright restrictions.

Gas hydrates (yellow) are ice with gas trapped inside; exposed beds are accessible to submersibles on the deep sea floor of the Gulf of Mexico. Ice worms, a new species only seen in hydrate, were discovered in 1997 by C. Fisher, Penn State University.
Credit: I. MacDonald

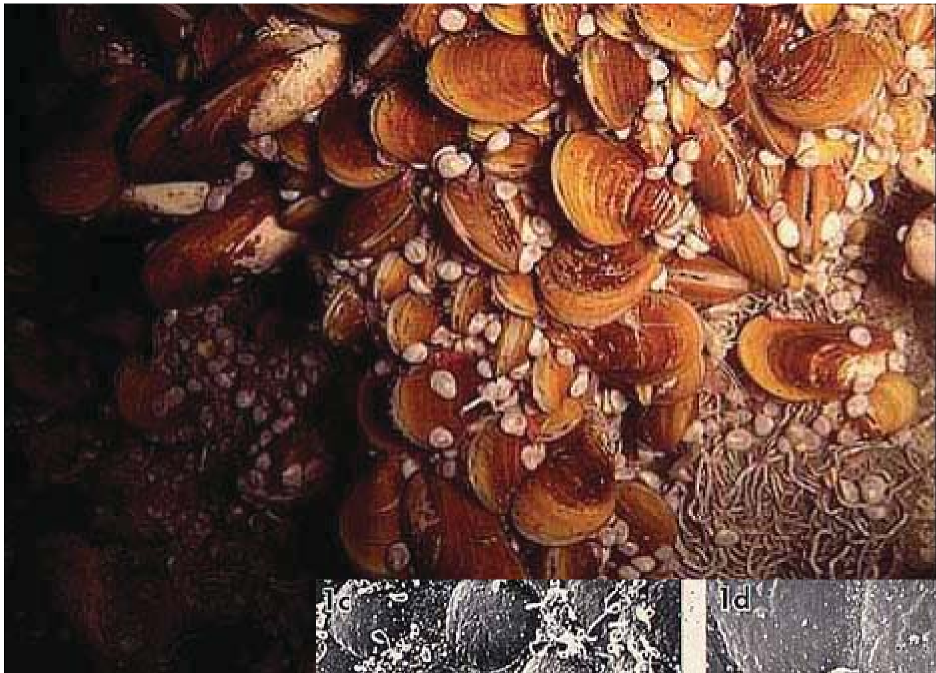

Methane-rich water is pumped into the mussel and across its gills. The symbiotic bacteria in the gills use methane as both a carbon and energy source. The mussels, in turn, live off the symbiotic bacteria.

Courtesy of Charles Fisher, Penn State University, Dept. of Biology. Used with permission.

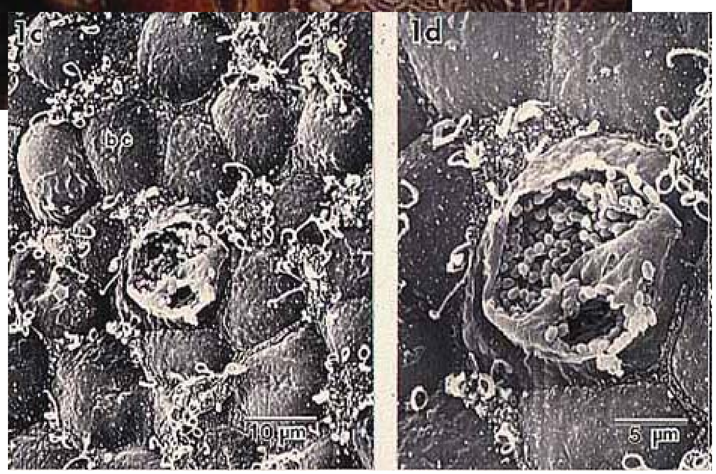

Using the scanning electron microscope, we can see over a dozen mussel gill cells in the panel on the left. On the right is a closer look at the cell with its outer membrane partially removed. Look into the cell to see hundreds of symbiotic bacteria.

APPLIED AND ENVIRONMENTAL MICROBIOLOGY, Feb. 1995, p. 576–582 Vol. 61, No. 2
0099-2240/95/$04.00+0

Identification of Methanotrophic Lipid Biomarkers in Cold-Seep Mussel Gills: Chemical and Isotopic Analysis

LINDA L. JAHNKE,[1*] ROGER E. SUMMONS,[2] LESLEY M. DOWLING,[2] AND KAREN D. ZAHIRALIS[1,3]

National Aeronautics and Space Administration, Ames Research Center, Moffett Field, California 94035-1000[1]; Australian Geological Survey Organisation, Canberra, ACT 2601, Australia[2]; and SETI Institute, Mountain View, California 94043[3]

Received 15 August 1994/Accepted 24 November 1994

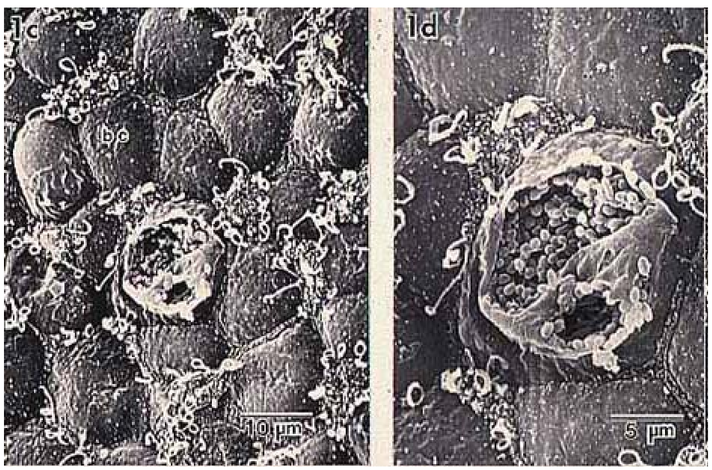

Table 3 removed due to copyright restrictions.

Using the scanning electron microscope, we can see over a dozen mussel gill cells in the panel on the left. On the right is a closer look at the cell with its outer membrane partially removed. Look into the cell to see hundreds of symbiotic bacteria.

Courtesy of Charles Fisher, Penn State University, Dept. of Biology. Used with permission.

Organic Geochemistry 39 (2008) 1659–1667

Contents lists available at ScienceDirect

Organic Geochemistry

journal homepage: www.elsevier.com/locate/orggeochem

Aerobic methanotrophy at ancient marine methane seeps: A synthesis

Daniel Birgel *, Jörn Peckmann

DFG-Forschungszentrum Ozeanränder, Universität Bremen, Postfach 330 440, 28334 Bremen, Germany

ARTICLE INFO

Article history:
Received 4 September 2007
Received in revised form 2 January 2008
Accepted 16 January 2008
Available online 20 February 2008

ABSTRACT

The molecular fingerprints of the chemosynthesis based microbial communities at methane seeps tend to be extremely well preserved in authigenic carbonates. The key process at seeps is the anaerobic oxidation of methane (AOM), which is performed by consortia of methanotrophic archaea and sulphate reducing bacteria. Besides the occurrence of ^{13}C depleted isoprenoids and *n*-alkyl chains derived from methanotrophic archaea and sul-

Table 1
Background information on samples

Location	Fossil inventory	Carbonate microfabrics	Stable isotopes	References
Tepee Buttes (Campanian)	Lucinid bivalves, gastropods	Clotted micrite, yellow calcite, banded/botryoidal cement, *in situ* brecciation	Yellow calcite $\delta^{13}C$:−45.9 to −31.7‰, micrite $\delta^{13}C$:−49.7 to −43.1‰, banded/botryoidal cement $\delta^{13}C$: −45.5 to −13.2‰	Kauffman et al., 1996; Shapiro, 2004; Birgel et al., 2006b
Pietralunga (Miocene)	Lucinid bivalves	Microcrystalline calcite, aragonitic cement, fossilized filaments	Microcrystalline calcite $\delta^{13}C$: −51.5 to −45.8‰, aragonitic cement $\delta^{13}C$: −43.3 to −40.8‰	Peckmann et al., 2004; Barbieri and Cavalazzi, 2005
Marmorito (Miocene)	None	Microcrystalline dolomite, calcitic veins, *in situ* brecciation	Microcrystalline dolomite $\delta^{13}C$: −40.7 to −38.9‰, calcitic vein $\delta^{13}C$: −28.5 to −17.3‰	Clari et al., 1988; Peckmann et al., 1999

$\delta^{13}C$ carbonate values in ‰ relative to V-PDB.

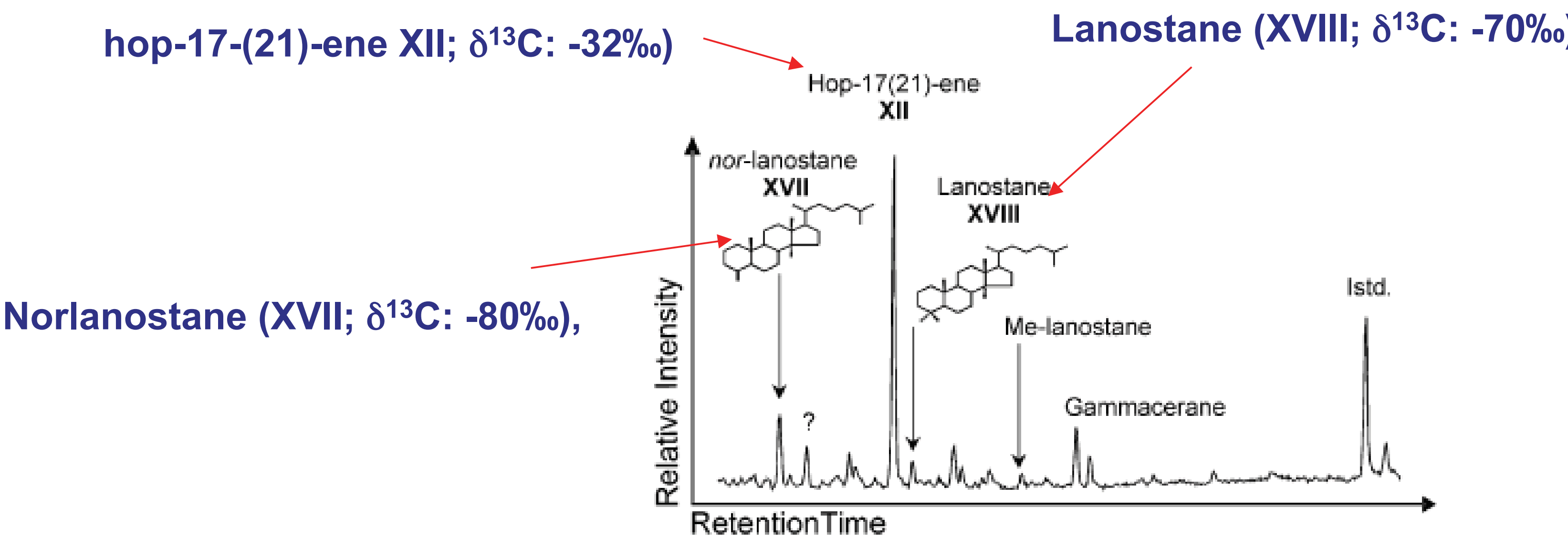

Fig. 1. Partial gas chromatogram (total Ion Current: TIC) of hydrocarbon fraction from Pietralunga. Istd.: internal standard. Roman numbers: see Appendix.

C-isotopic Composition of Organic Compounds

- Fractionation during biosynthesis (lipids)

DeNiro and Epstein, 1977

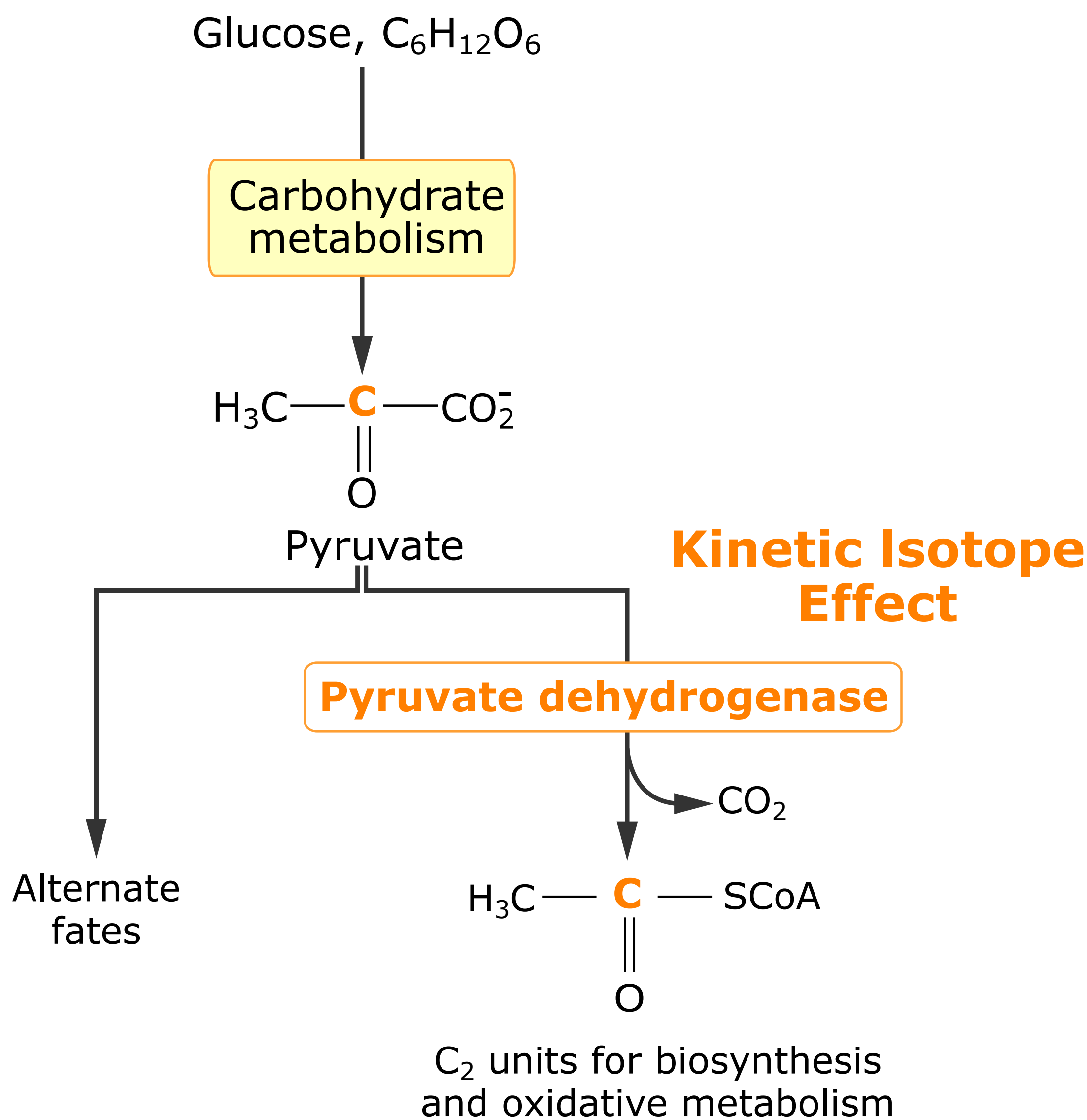

Image by MIT OpenCourseWare.

m c

Precursor = Acetate: $CH_3{-}CO_2^{-}$

Product = C_{16} fatty acid = 8 acetates

m c m c m c m c m c m c m c m c

$CH_3{-}CH_2{-}CH_2{-}CH_2{-}CH_2{-}CH_2{-}CH_2{-}CH_2{-}CH_2{-}CH_2{-}CH_2{-}CH_2{-}CH_2{-}CH_2{-}CH_2{\cdot}CO_2H$

Methyl (m) and carboxyl (c) positions in acetate are converted to structurally equivalent CH_2 positions during biosynthesis m c m c m c m c m c m c m c m c

$CH_3-CH_2-CH_2-CH_2-CH_2-CH_2-CH_2-CH_2-CH_2-CH_2-CH_2-CH_2-CH_2-CH_2-CH_2\cdot CO_2H$

Isotopic equilibrium:

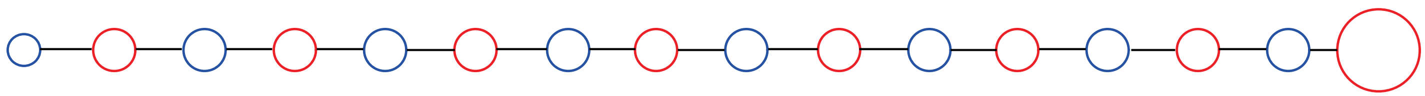

Equilibration within acetate → 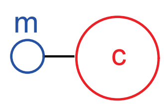

Biosynthesis without subsequent equilibration →

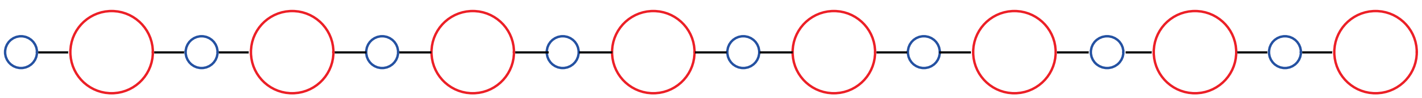

Kinetic control throughout, acetate = 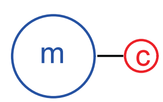

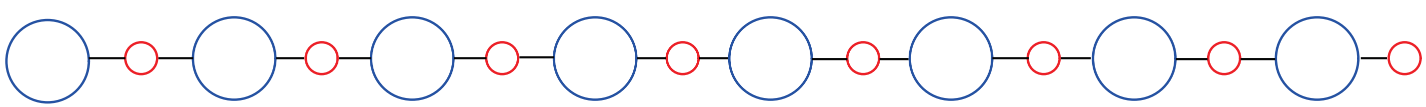

These images have been removed due to copyright restrictions.

Flows of C at the pyruvate branch point in the metabolism of E. coli grown aerobically on glucose (Roberts 1955). 74% of the pyruvate is decarboxylated to yield Ac-CoA. The observed depletion at odd-numbered positions of FAcids is shown at the right indicating that the isotope effect at C-2 in the pyruvate dehydrogenase reaction is 23‰

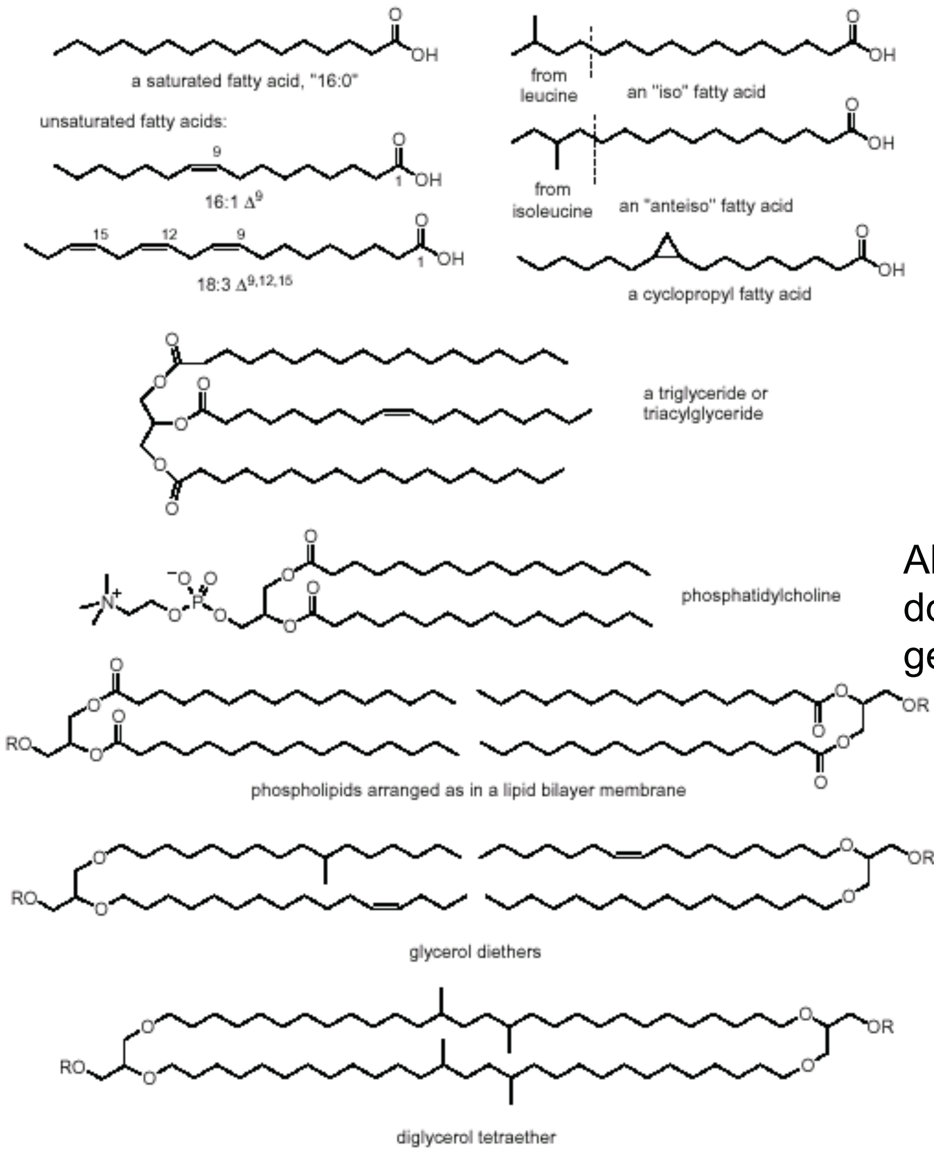

An important consequence of the pyruvate to acetate isotopic fractionation

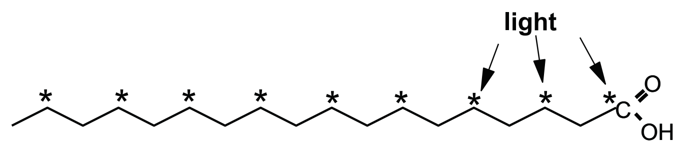

Alternate carbons derived from acetate carboxyl down acetogenic lipidbackbones are light. In general lipids are also light, but not as light.

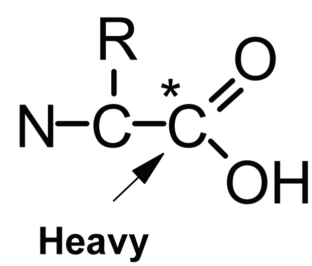

In contrast, the carboxyl carbon of amino acids is generally "heavy"

Two Origins for Isoprenoids

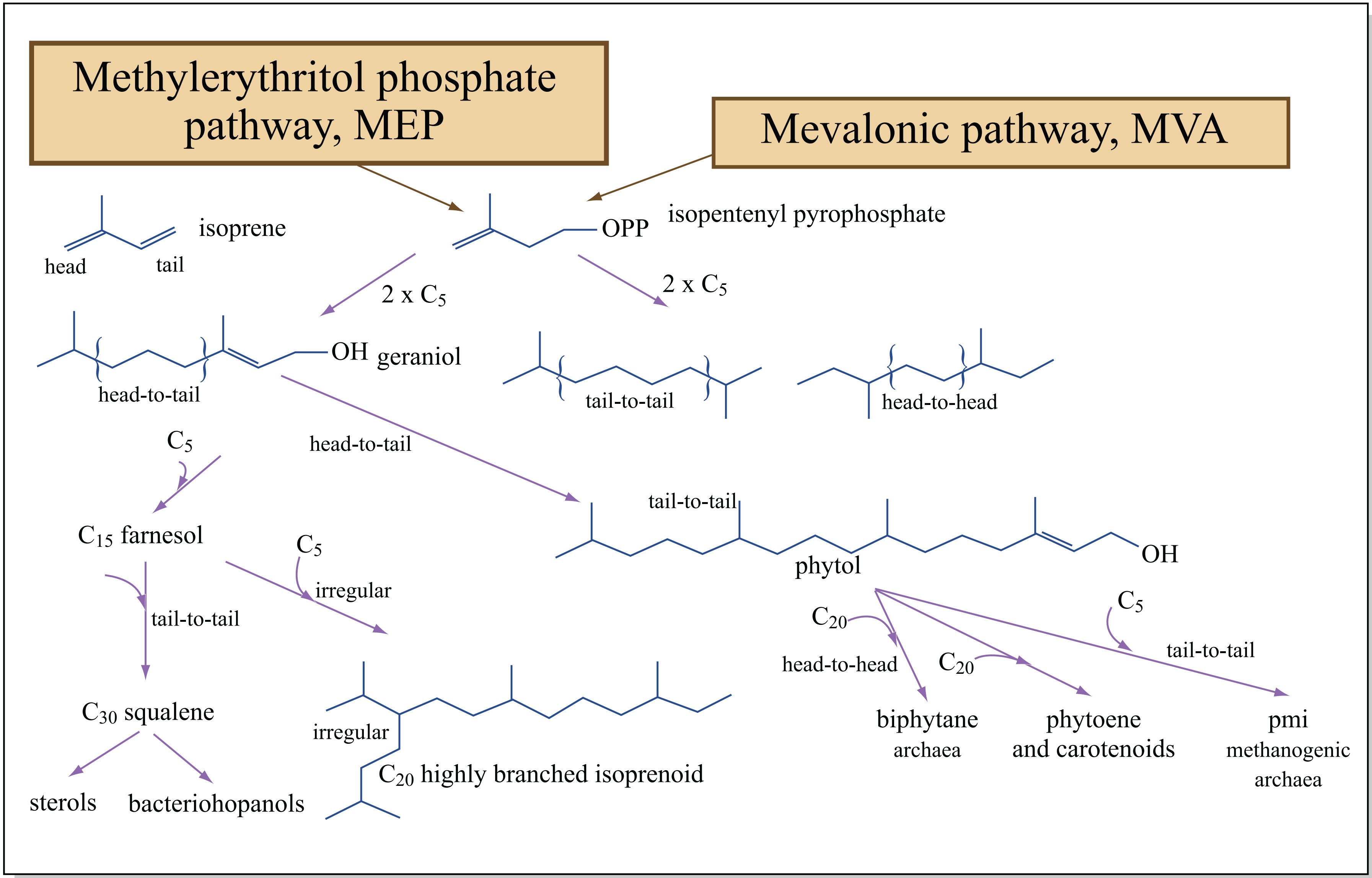

Figure by MIT OpenCourseWare.

Labelling of isopentenylpyrophosphate from MVA pathway

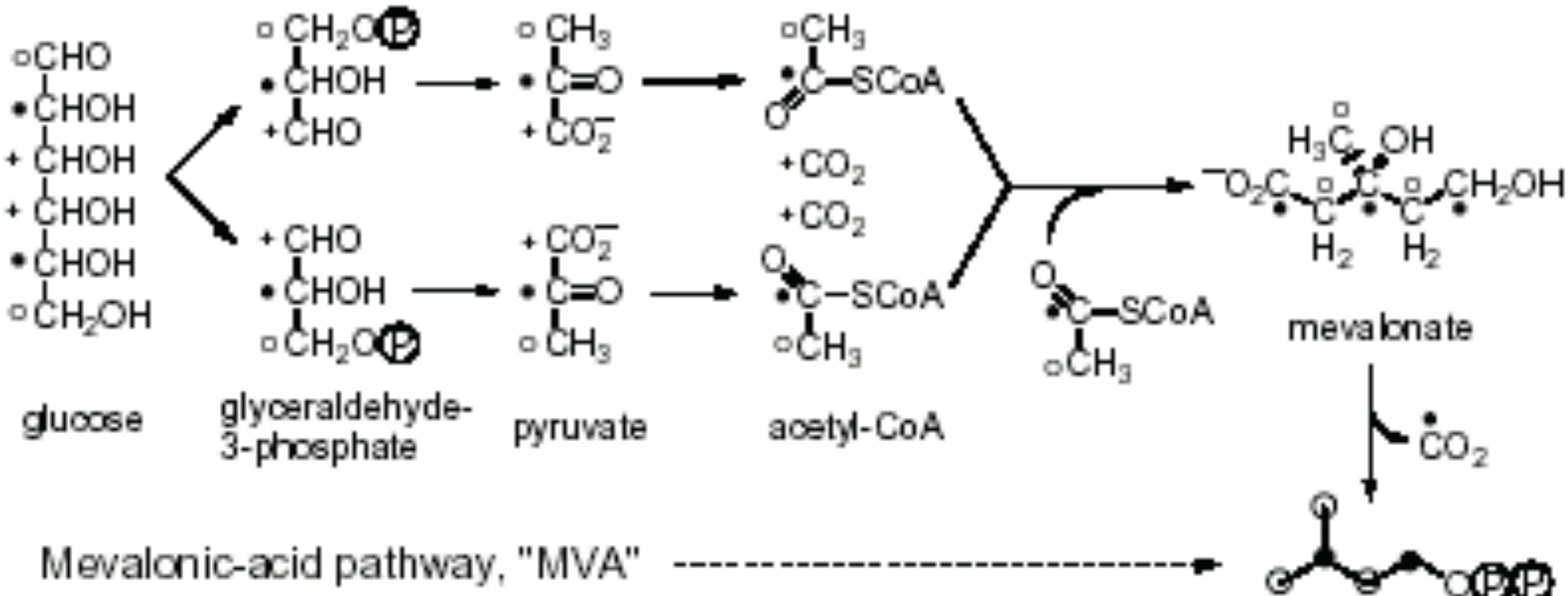

Labelling of isopentenylpyrophosphate from MEP pathway

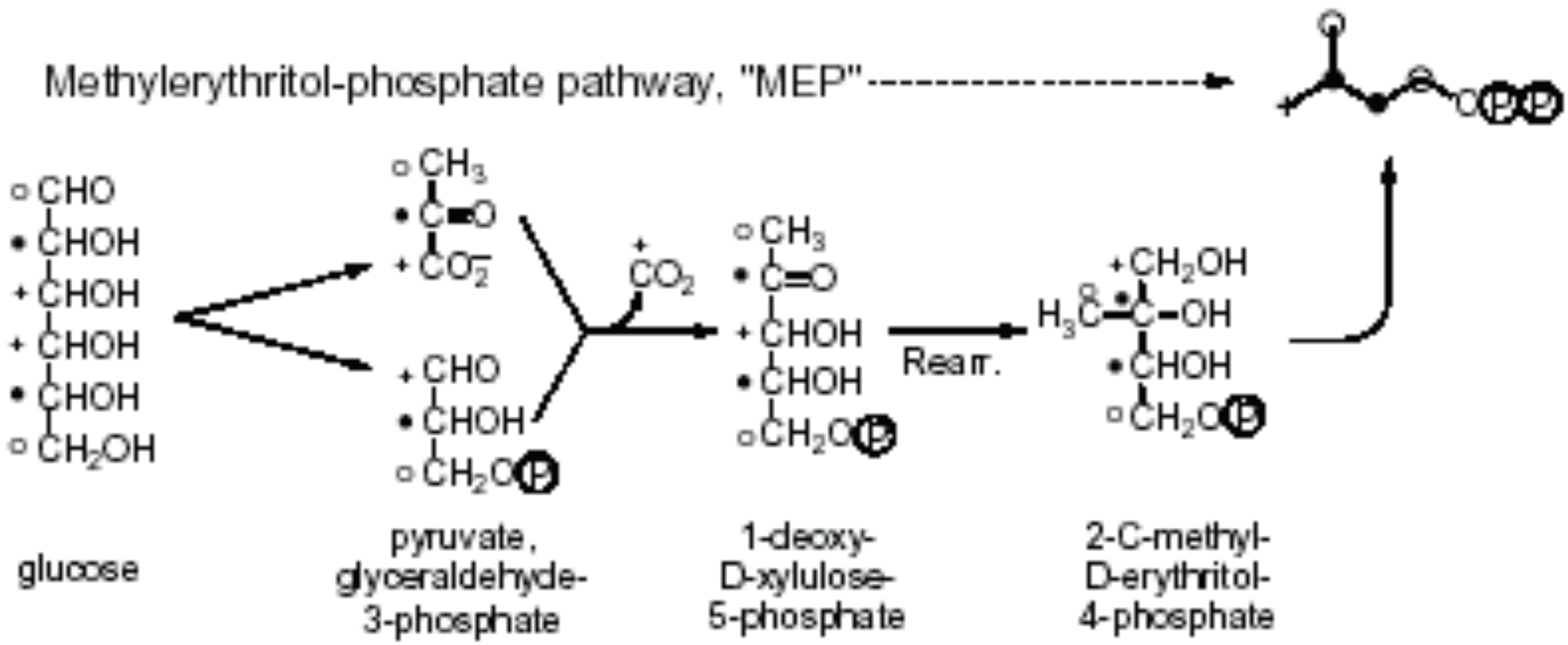

Labeling of phytol and cholesterol from MVA (a & c) and MEP (b & d)

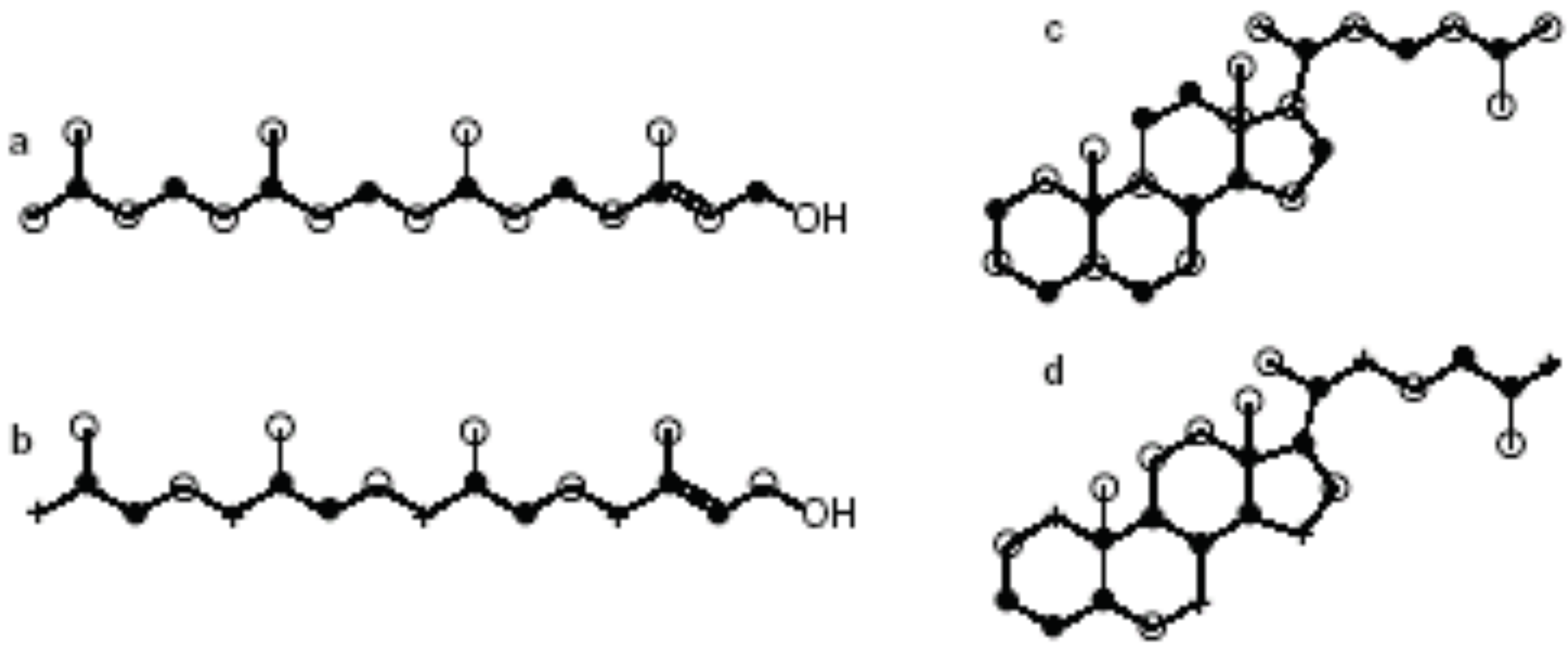

Pathways Used for The Biosynthesis of Isoprenoid Lipids.

Organism	Pathway		Reference
Prokaryotes	-		Lange *et al*., 2000
Bacteria	-		Boucher and Doolittle, 2000
Aquificales, Thermotogales	MEP		-
Photosynthetic bacteria	-		-
Chloroflexus	MVA		Rieder *et al*., 1998
Chlorobium	MEP		Boucher and Doolittle, 2000
Gram positive eubacteria	-		-
Commonly	MEP		-
Streptococcus, Staphylococcus	MVA		Boucher and Doolittle, 2000
Streptomyces	MEP & MVA		Seto *et al*., 1996
Spirochaetes	-		Boucher and Doolittle, 2000
Borrelia burgdorferi	MVA		-
Treponema pallidum	MEP		-
Proteobacteria	-		-
Commonly	MEP		-
Myxococcus, Nannocystis	MVA		Kohl *et al*., 1983
Cyanobacteria	MEP		Disch *et al*., 1998
Archaea	MVA		Lange *et al*., 2000
Eukaryotes	-		-
Non-plastid-bearing	MVA		Lange *et al*., 2000
Plastid-bearing	Plastid	Cytosol	-
Chlorophyta	MEP	MEP	Schwender *et al*., 2001
Streptophyta	MEP	MVA	Lichtenthaler *et al*., 1997
Euglenoids	MVA	MVA	Lichtenthaler 1999

Image by MIT OpenCourseWare.

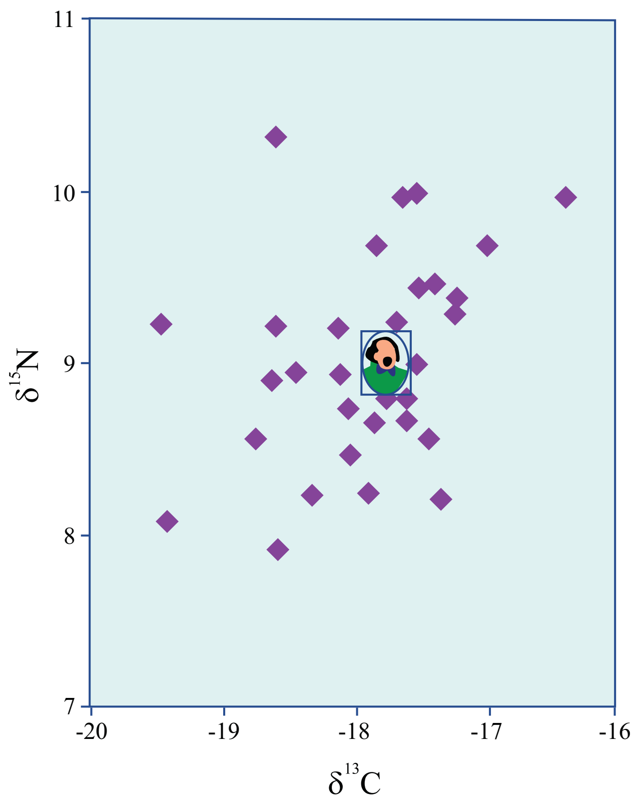

Twin element stable isotope distributions ($\delta^{13}C$ and $\delta^{15}N$, in ‰ versus PDB and air, respectively) of hair samples taken from individual students at the University of Virginia (modified after *Macko et al*. [1998]). Hair is largely composed of the fibrous protein α-keratin. Its isotope composition is reflective of the recent diet of an individual, generally increasing slightly (1‰ in $\delta^{13}C$ and 3‰ in $\delta^{15}N$) with tropic level. The marked variability accords with the great diversity of modern diets. For comparison, George Washington's hair sample testifies to a rather balanced diet.

Figure by MIT OpenCourseWare.

Multi-element, Compound-specific Isotopic Analyses **Vanillin**

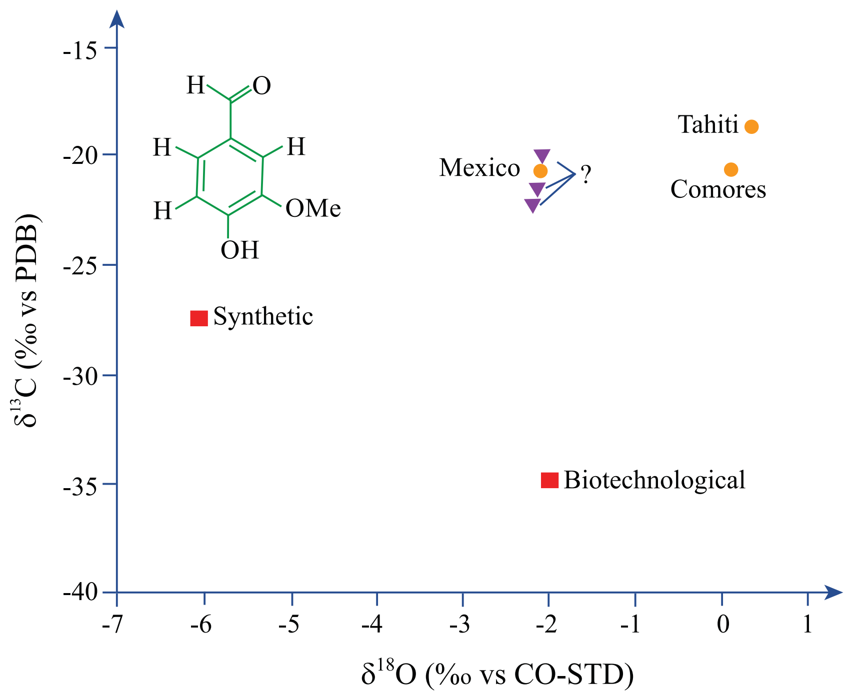

Dual isotopic ($\delta^{13}C$ and $\delta^{18}O$, in ‰ versus PDB and of standard CO, respectively) for the flavor compound vanillin. The three vanillin extracts from the naturally grown vanilla beans have similar $\delta^{13}C$ values, even though they come from geographically widely spaced sites: Mexico and the islands of the Comores and Tahiti. The Mexican sample, however, does differ markedly in $\delta^{18}O$, no doubt owing to major differences in $\delta^{18}O$ in the ambient water supply. Not surprisingly, major differences in both $\delta^{13}C$ and $\delta^{18}O$ are apparent in the synthetic and biotechnological products [*Hener et al., 1998*]. On the basis of their dual isotopic values, the three samples of unknown origin can be assigned to Mexico.

Figure by MIT OpenCourseWare.

Characterising Cocaine Sources

These images have been removed due to copyright restrictions.

Figure 2. Identification of geographic regions in South America where coca is commonly grown, based on dual isotope information of cocaine base as well as abundance of minor alkaloid components. Plotted on both axes are mixed expressions, each consisting of an isotope term and a concentration term; the *y* axis is [δ^{15}N cocaine (‰ versus air) + 0.1 × relative concentration of truxilline (‰)], and the *x* axis is [δ^{13}C cocaine (‰ versus PDB) − 10 × concentration of trimethoxycocaine]. Truxilline and trimethoxycocaine occur as two trace alkaloids in coca leaves. In addition to the obvious benefits for forensics, this illustration demonstrates the potential value of multi-isotope biomarker approaches for the geosciences to distinguish different geographical, climatological, and ecological regimes. Furthermore, it illustrates the importance of innovative data manipulation in biomarker research, especially when multiple isotope dimensions are employed. After *Ehleringer et al.* [2000].

Multi-element, Compound-specific Isotopic Analyses

Vanillin

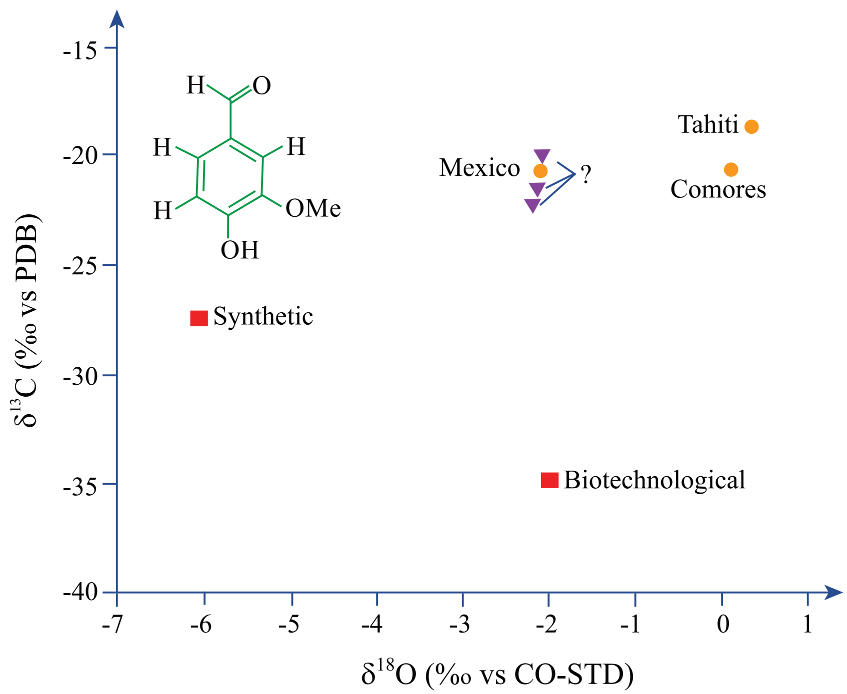

Dual isotopic ($\delta^{13}C$ and $\delta^{18}O$, in ‰ versus PDB and of standard CO, respectively) for the flavor compound vanillin. The three vanillin extracts from the naturally grown vanilla beans have similar $\delta^{13}C$ values, even though they come from geographically widely spaced sites: Mexico and the islands of the Comores and Tahiti. The Mexican sample, however, does differ markedly in $\delta^{18}O$, no doubt owing to major differences in $\delta^{18}O$ in the ambient water supply. Not surprisingly, major differences in both $\delta^{13}C$ and $\delta^{18}O$ are apparent in the synthetic and biotechnological products [*Hener et al., 1998*]. On the basis of their dual isotopic values, the three samples of unknown origin can be assigned to Mexico.

Figure by MIT OpenCourseWare.

Reservoirs of carbon in the Atmosphere, Hydrosphere and Geosphere.

Reservoir	Reduced C	Mass, x 10^{18} moles Oxidized C	Total C
Atmosphere	-	0.06[a]	0.06[a]
Biosphere: plants and algae	0.13[b]	-	0.13
Hydrosphere	-	3.3[c]	3.3
Pelagic sediments	60[d]	1300[d]	1360
Continental margin sediments	>370[e]	>1000[e]	>1370
Sedimentary rocks	750[f]	3500[f]	4250
Crustal metamorphic and igneous rocks	100[g]	?	>100
Mantle	-	-	27000[h]

a- Holland (1984). b- Mopper and Degens (1979); Olson et al. (1985). c- Holland (1984).
d- Holser, et al. (1988). e- Minimum inventories required for C isotopic mass balance.
f- Ronov (1980). g- Hunt (1972). h- Derived from estimates of mantle mass and C concentration.

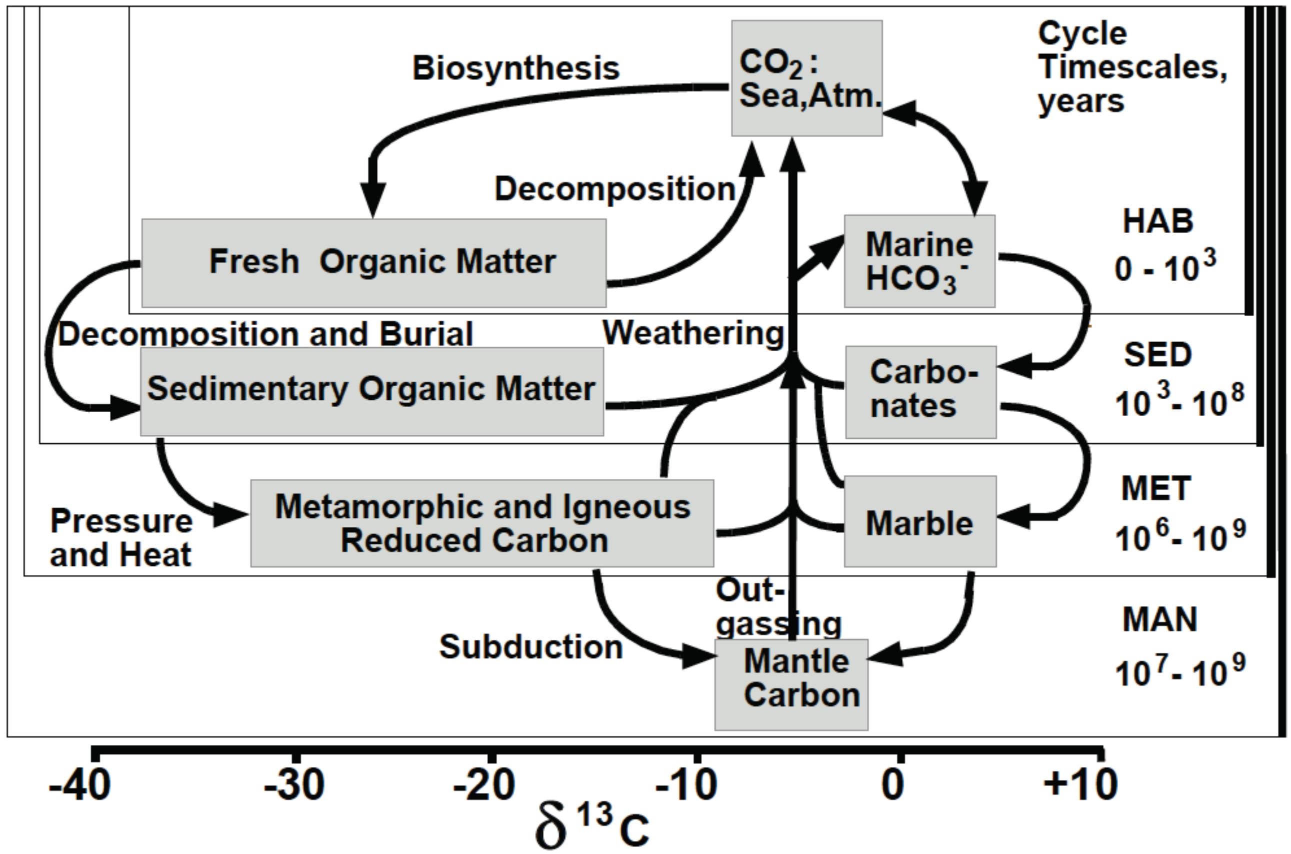

Figure 1. Biogeochemical C cycle, showing principal C reservoirs (boxes) in the mantle, crust, oceans and atmosphere, and showing the processes (arrows) that unite these reservoirs. The range of each of these reservoir boxes along the horizontal axis gives a visual estimate of δ13C values most typical of each reservoir. The vertical bars at right indicate the timeframes within which C typically completely traverses each of the four C sub-cycles (the HAB, SED, MET and MAN sub-cycles, see text). For example, C can traverse the hydrosphere-atmosphere-biosphere (HAB) sub-cycle typically in the time scale between 0 to 1000 years.

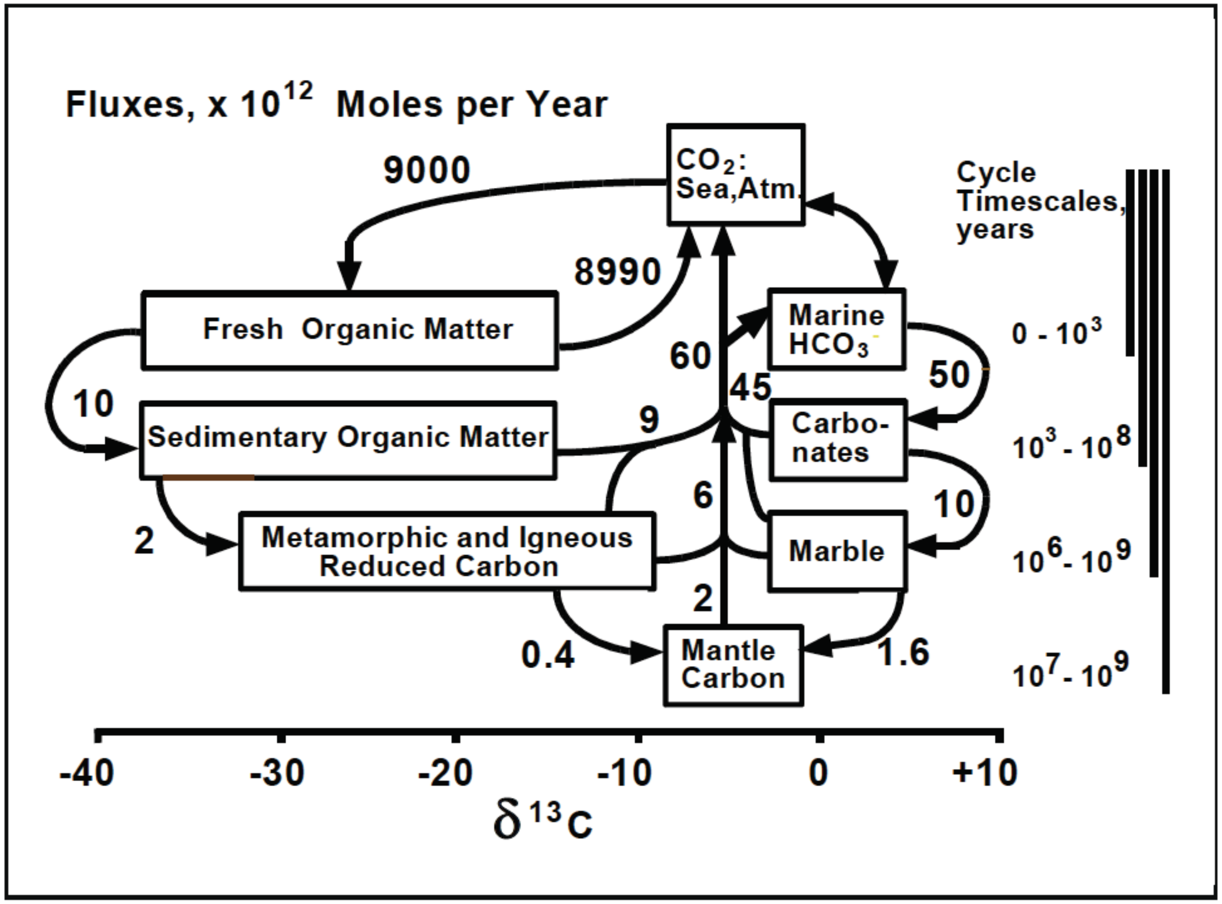

Image courtesy of Mineralogical Society of America. Used with permission.

Figure 2. Biogeochemical C cycle (as in Fig. 1), showing principal C reservoirs (boxes) and their isotopic compositions in the mantle, crust, oceans and atmosphere, and the processes (arrows) that unite these reservoirs. Numbers adjacent to the arrows give estimates of present-day fluxes, expressed in the units 10^{12} mol yr-1.

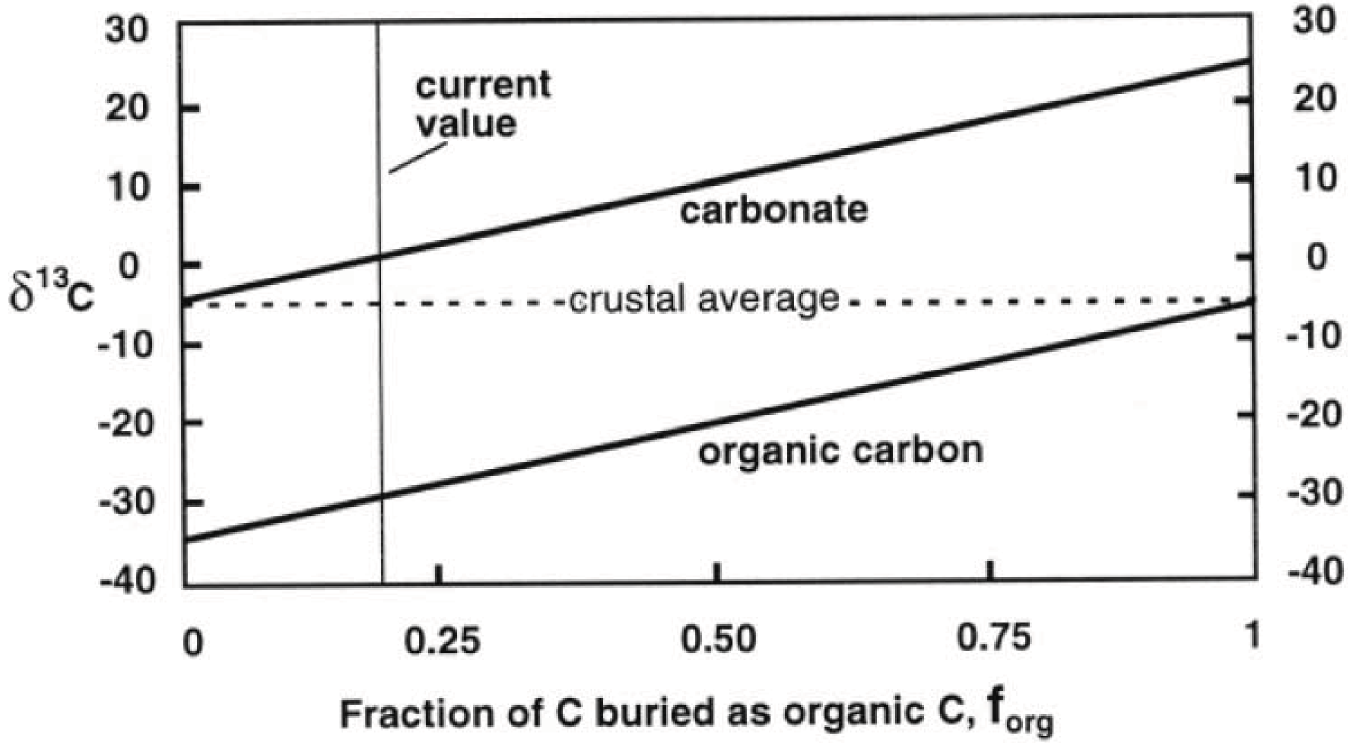

Figure 3. Relationship between isotopic composition (**δcarb and δorg)** and the fraction of carbon buried as organic matter. The vertical separation between the lines depicts **εΔ, and thus reflects the combined** effects of equilibria between inorganic C species and biological isotope discrimination (see text). A value **εTOC = 30 is depicted here, and** represents the long-term average value during the past 800 Ma (Hayes et al. 1999). The vertical line represents the value of forg = 0.2, which represents the current value for the global C cycle.

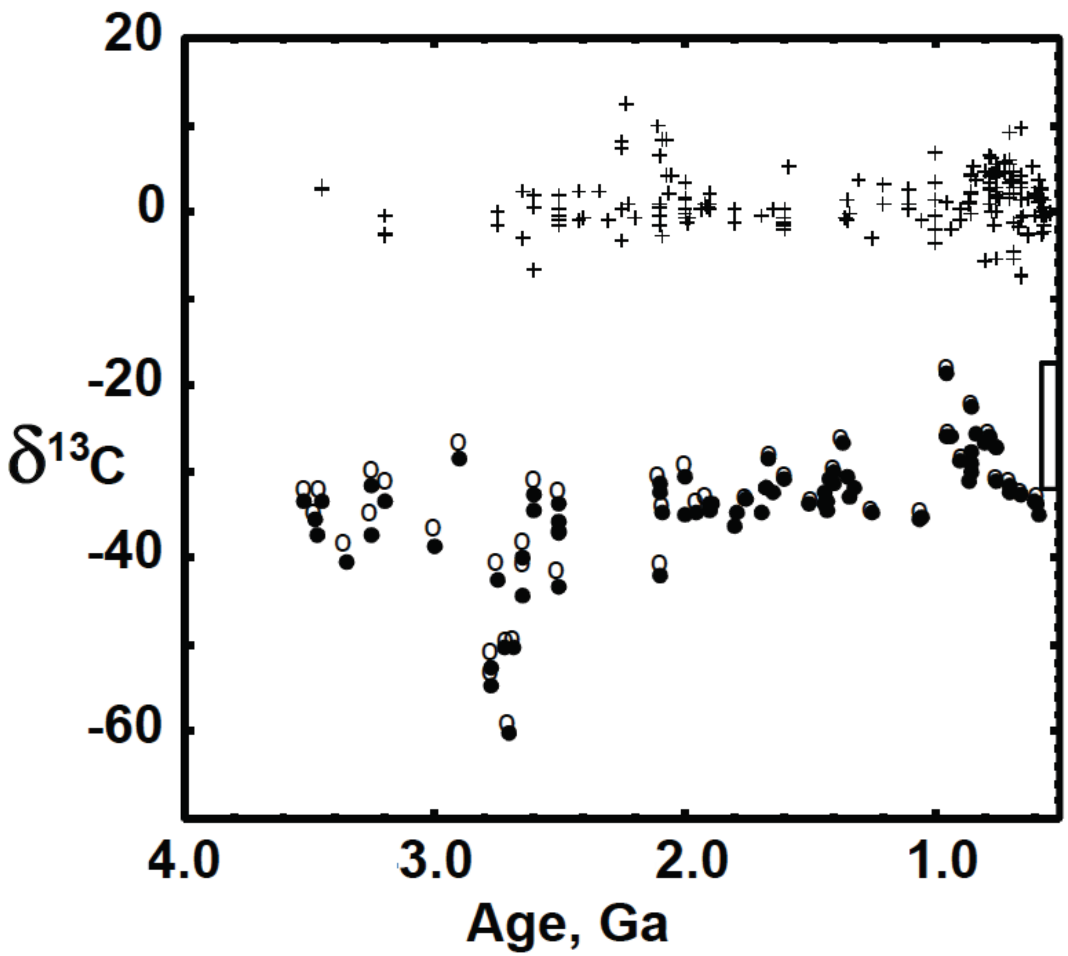

Figure 5. Plot of age versus **δcarb (crosses) and δorg for Archean and** Proterozoic kerogens. Kerogen data (filled circles) are corrected for the effects of thermal alteration (Des Marais 1997a). Uncorrected data are shown as open circles. Between 2.2 to 2.0 billion years ago, note the high **δcarb values and the virtual disappearance thereafter of δorg values** more negative than -36. Other evidence indicates that atmospheric O2 increased substantially at this time (see text).

Secular variation in $\delta^{13}C$ of purified kerogens (sedimentary organic matter)

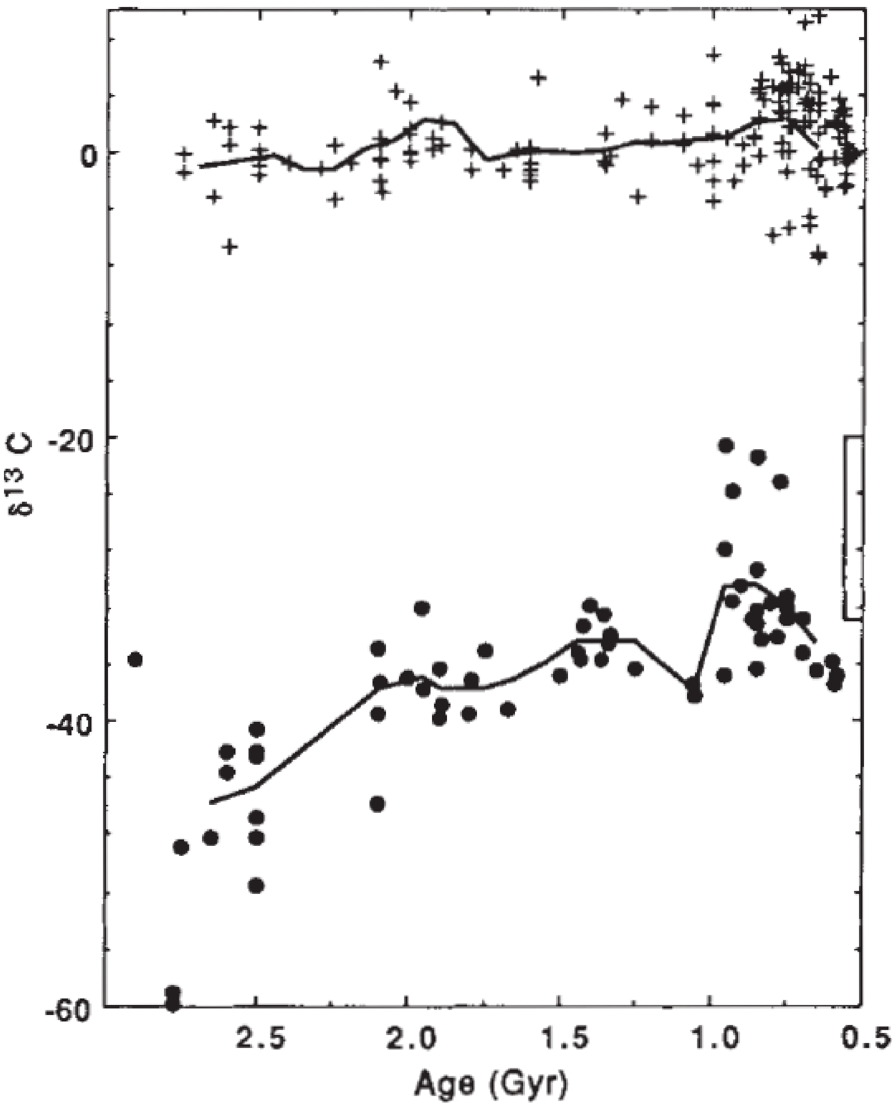

Carbon isotope evidence for the stepwise oxidation of the Proterozoic environment

David J. Des Marais*, Harald Strauss†, Roger E. Summons‡ & J. M. Hayes§

* NASA, Ames Research Center, Moffett Field, California 94035, USA
† Institut für Geologie, Ruhr-Universität Bochum, Postfach 102148, 4630 Bochum 1, Germany
‡ Bureau of Mineral Resources, GPO Box 378, Canberra, Australian Capital Territories 2605, Australia
§ Biogeochemical Laboratories, Departments of Geological Sciences and of Chemistry, Geology Building, Indiana University, Bloomington, Indiana 47405, USA

The oxidation of the Earth's crust and the increase in atmospheric oxygen early in Earth history have been linked to the accumulation of reduced carbon in sedimentary rocks. Trends in the carbon isotope composition of sedimentary organic carbon and carbonate show that during the Proterozoic aeon (2.5–0.54 Gyr ago) the organic carbon reservoir grew in size, relative to the carbonate reservoir. This increase, and the concomitant release of oxidizing power in the environment, occurred mostly during episodes of global rifting and orogeny.

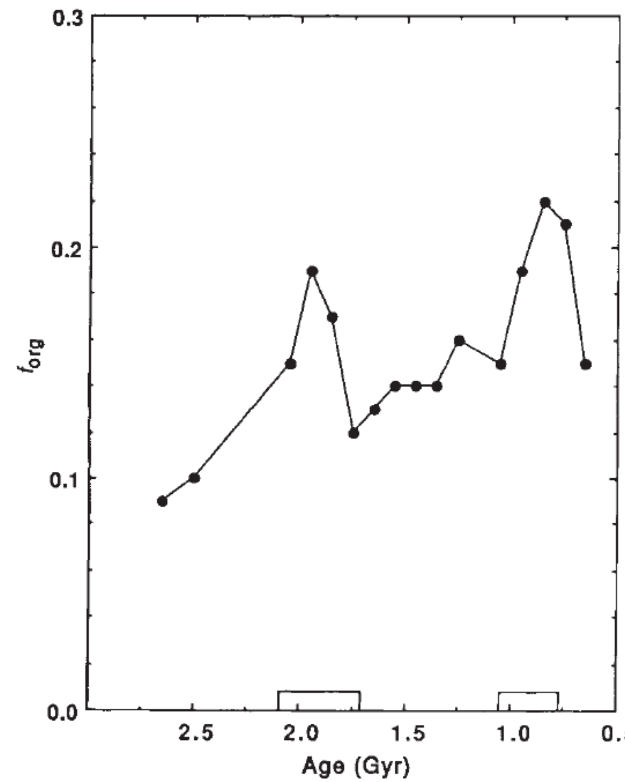

Fraction of carbon buried as organic matter

Reprinted by permission from Macmillan Publishers Ltd: Nature.
Source: David J. Des Marais, Harald Strauss, Roger E. Summons, J.M. Hayes. "Carbon Isotope Evidence for the Stepwise Oxidation of the Proterozoic environment." *Nature* 359 (1992): 605–9. doi:10.1038/359605a0.

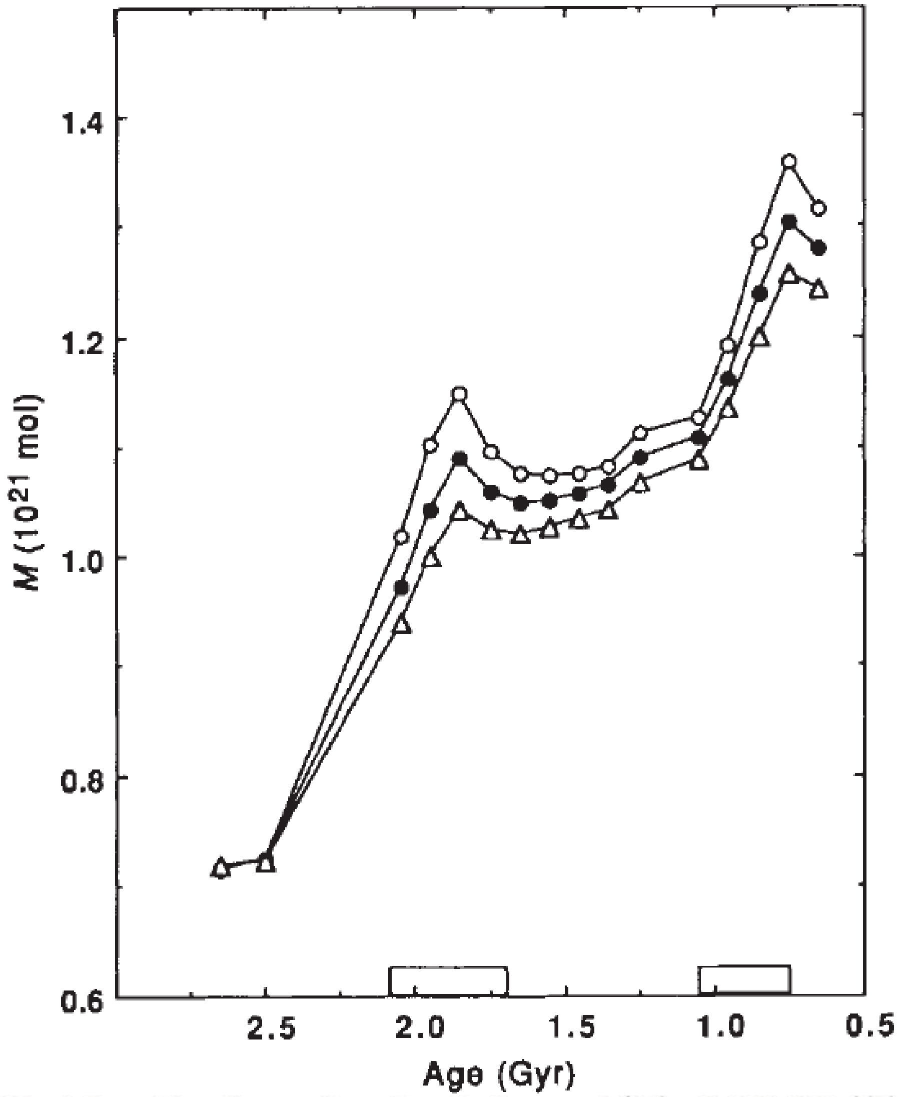

FIG. 4 Quantity of organic carbon in the crust (M) against age. Values of M are calculated according to equation (4) (in the text). Symbols represent calculations of M, assuming sediment half lives (see derivation of equation (4) as follows : ○, 300 Myr; ●, 400 Myr; △, 500 Myr. Rectangles along the bottom margin depict time intervals of enhanced global rifting and orogeny (see text).

Carbon isotope evidence for the stepwise oxidation of the Proterozoic environment

David J. Des Marais*, Harald Strauss†, Roger E. Summons‡ & J. M. Hayes§

* NASA, Ames Research Center, Moffett Field, California 94035, USA
† Institut für Geologie, Ruhr-Universität Bochum, Postfach 102148, 4630 Bochum 1, Germany
‡ Bureau of Mineral Resources, GPO Box 378, Canberra, Australian Capital Territories 2605, Australia
§ Biogeochemical Laboratories, Departments of Geological Sciences and of Chemistry, Geology Building, Indiana University, Bloomington, Indiana 47405, USA

The oxidation of the Earth's crust and the increase in atmospheric oxygen early in Earth history have been linked to the accumulation of reduced carbon in sedimentary rocks. Trends in the carbon isotope composition of sedimentary organic carbon and carbonate show that during the Proterozoic aeon (2.5–0.54 Gyr ago) the organic carbon reservoir grew in size, relative to the carbonate reservoir. This increase, and the concomitant release of oxidizing power in the environment, occurred mostly during episodes of global rifting and orogeny.

Source: David J. Des Marais, Harald Strauss, Roger E. Summons, J.M. Hayes. "Carbon Isotope Evidence for the Stepwise Oxidation of the Proterozoic environment." *Nature* 359 (1992): 605–9. doi:10.1038/359605a0.

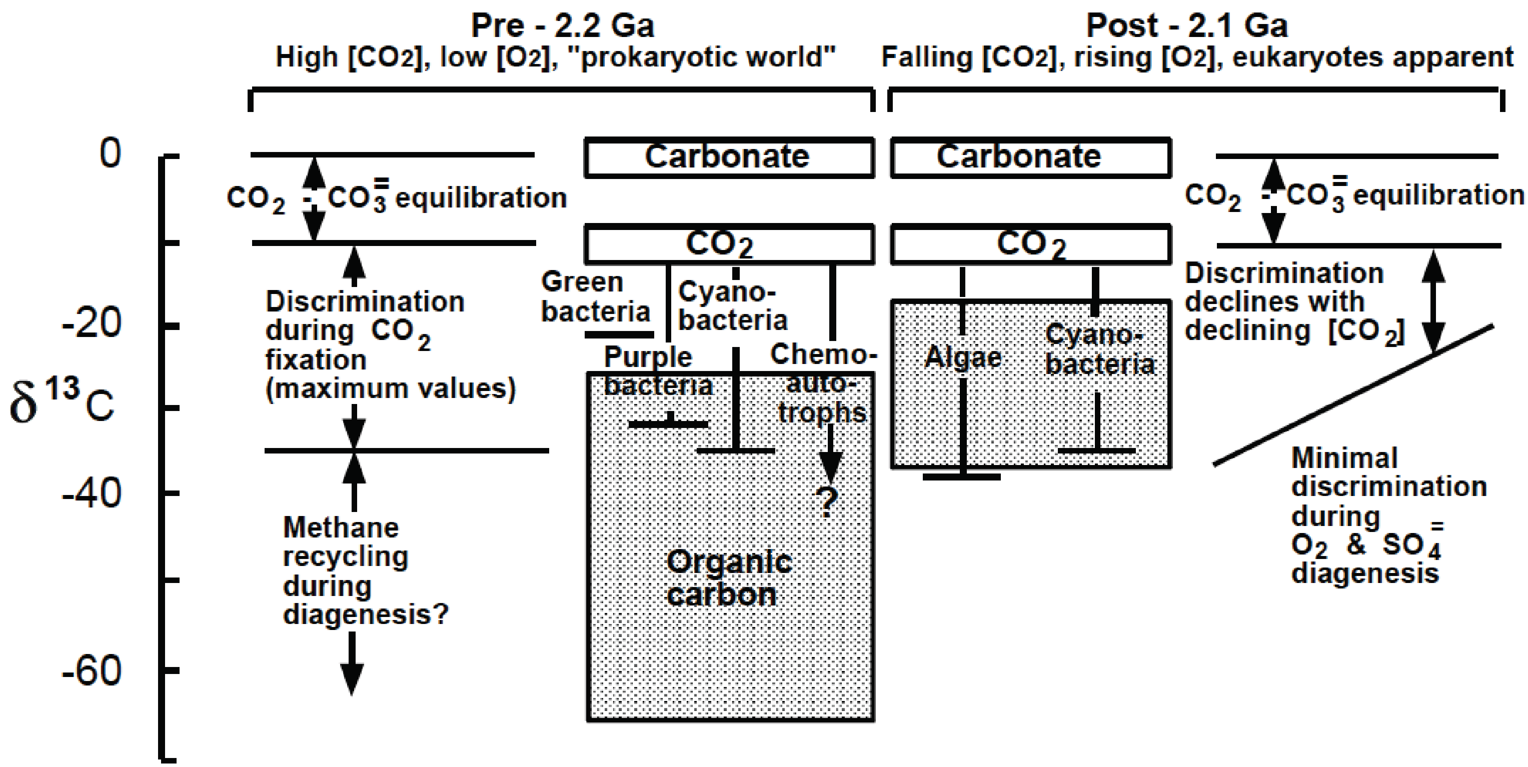

Figure 8. Range of **δcarb and δCO2 values (open boxes) and δorg values (shaded boxes), together** with the processes proposed to explain their distribution prior to 2.2 Ga and subsequent to 2.1 Ga. A temperature of 15°C was assumed for the isotopic equilibrium between **δcarb and δCO2. The lines** associated with the various groups of autotrophic bacteria and algae illustrate the maximum discrimination expected for each group. The sloped line at right depicts declining discrimination over time, perhaps in response to declining CO2 levels.

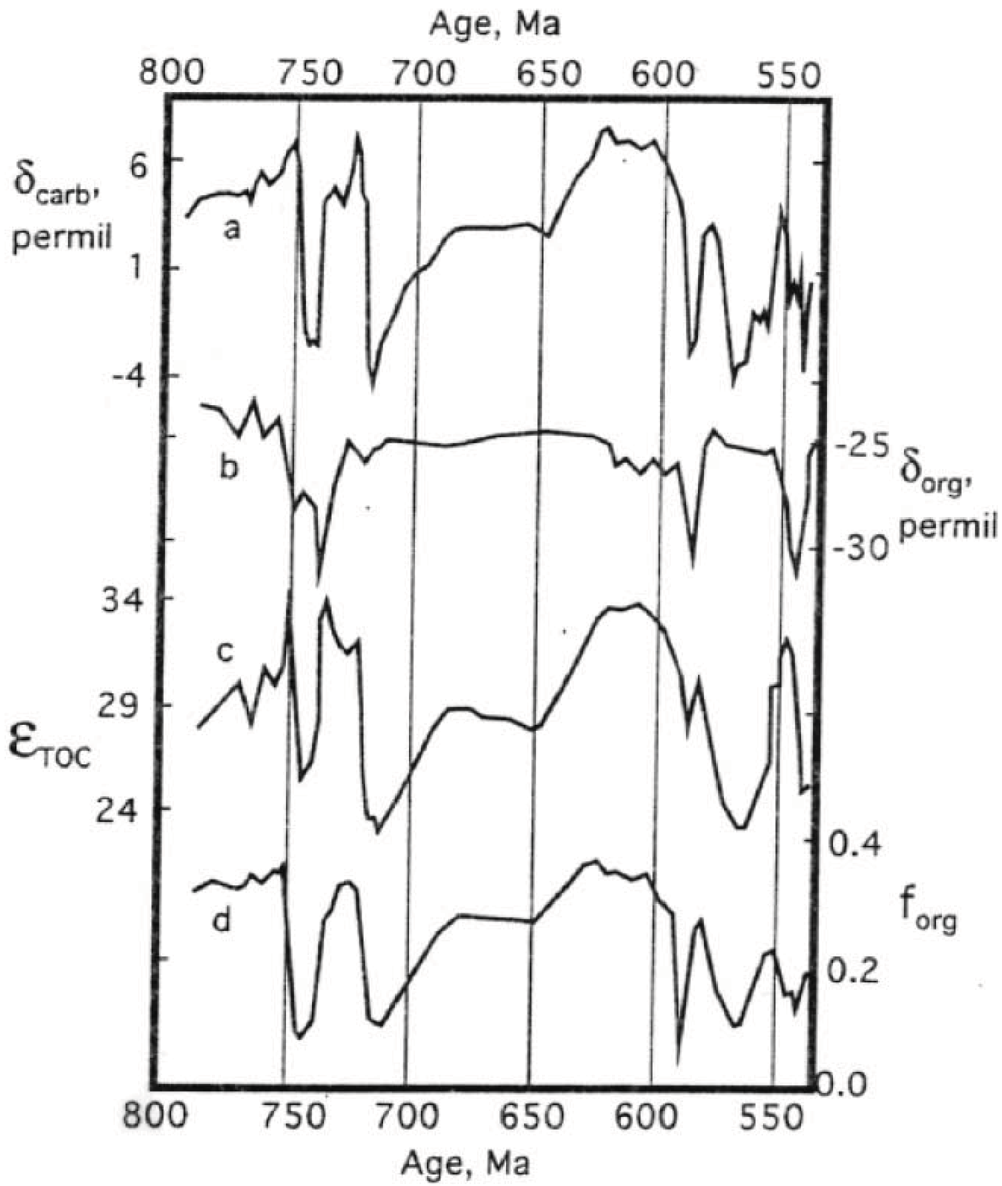

Image courtesy of Mineralogical Society of America. Used with permission.

Figure 11. Neoproterozoic records of **δcarb (curve a) and δorg (curve b)** values (Hayes et al. 1999). Corresponding values for isotopic fractionation, **εTOC and forg during Neoproterozoic** time are given by curves c and d, respectively. The periodic negative excursions are typically associated with glacial intervals (see text). Figure modified from Hayes et al. (1999).

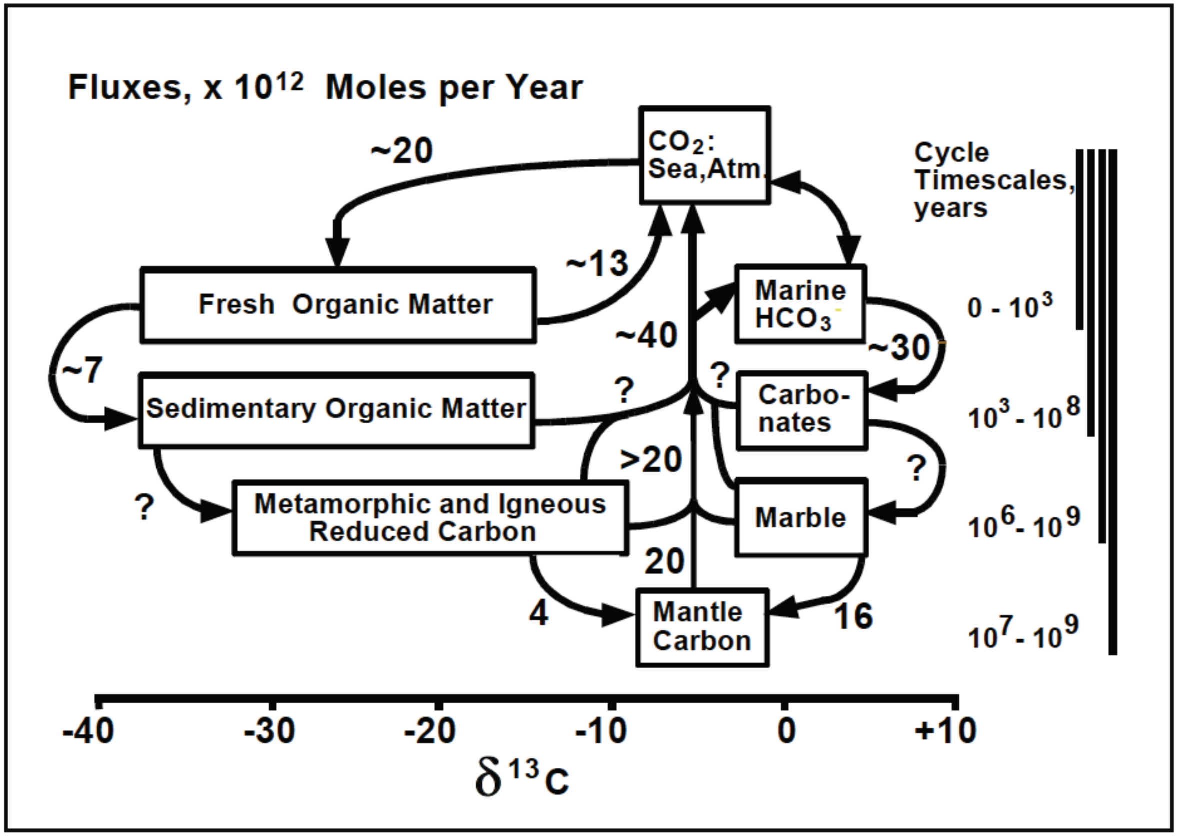

Figure 7. The biogeochemical C cycle prior to the advent of oxygenic photosynthesis, showing the much lower global primary productivity and the higher rates of thermal emanation of C (see text). Comparison with Figure 5 illustrates the enhancement of global primary productivity due to the development of oxygenic photosynthesis. Flux estimates are highly approximate, and are shown principally to illustrate the direction and magnitude of change over geologic time.

Biosynthesis of Organic Compounds

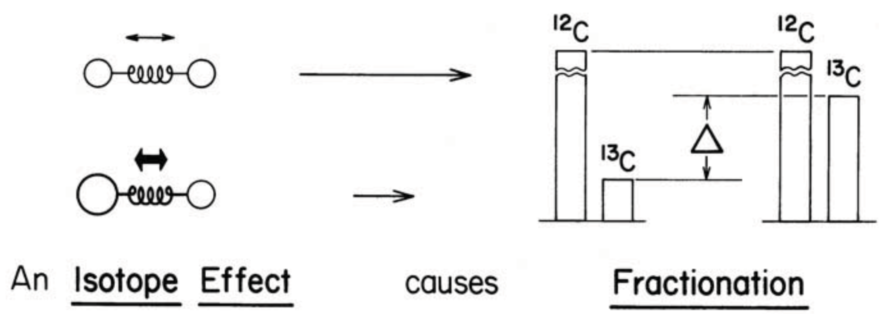

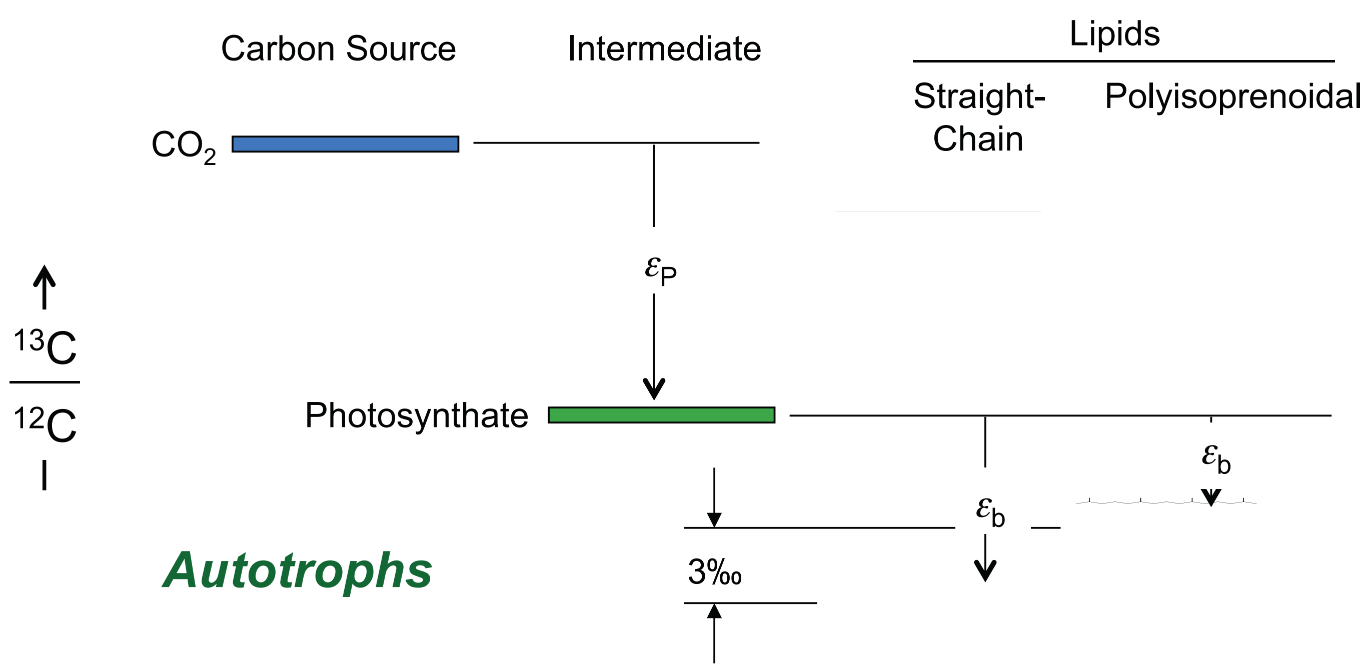

Biosynthesis of Organic Compounds

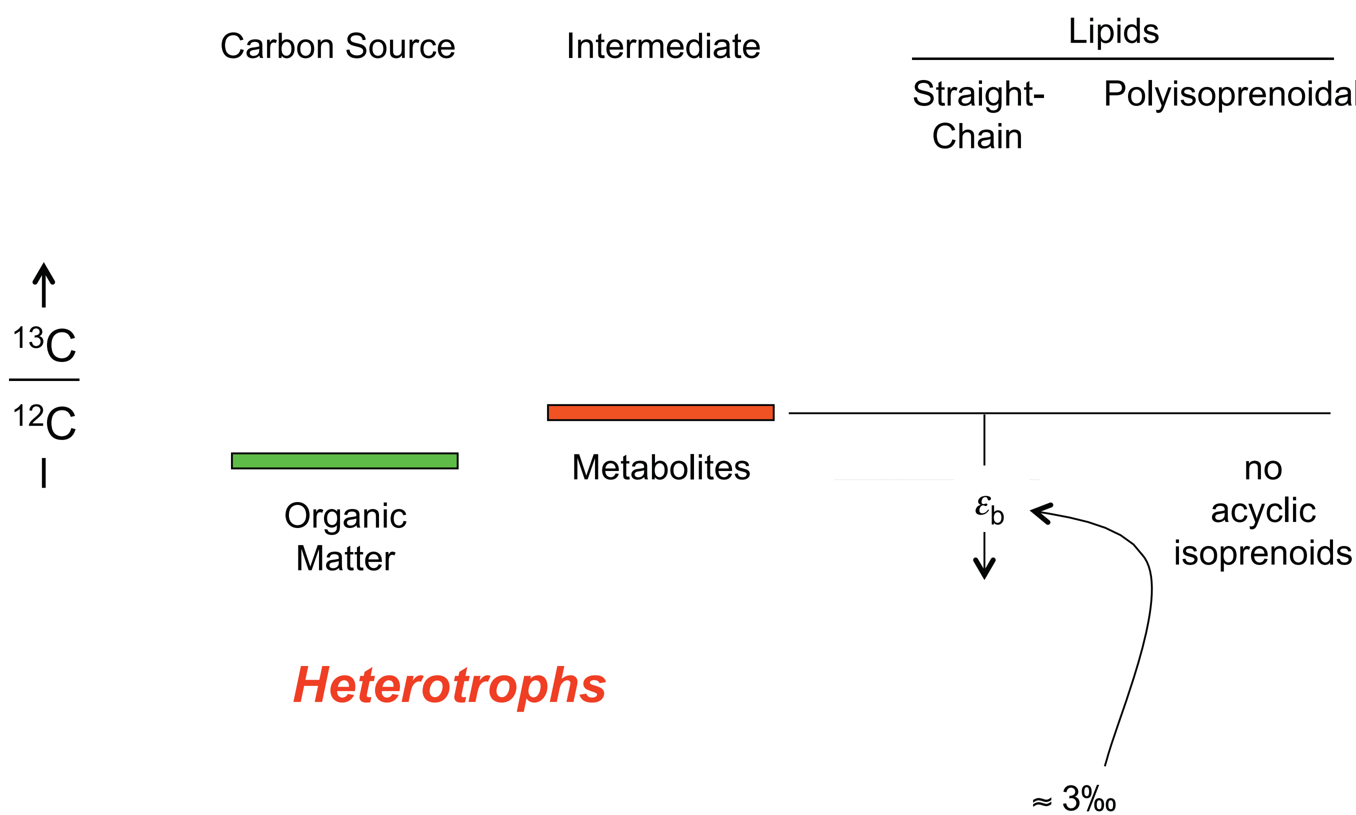

Heterotrophs

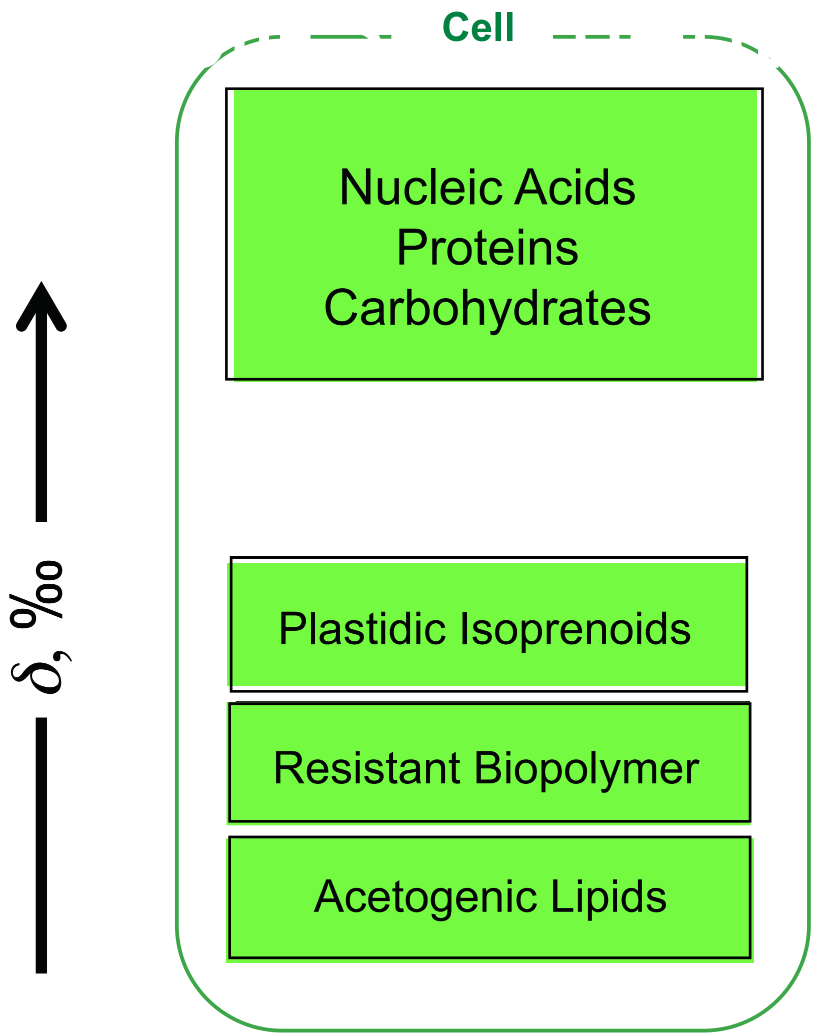
Cell
Nucleic Acids
Proteins
Carbohydrates
Plastidic Isoprenoids
Resistant Biopolymer
Acetogenic Lipids
δ, ‰

12.007 Geology
Spring 2013